10034–10051 *Nucleic Acids Research, 2018, Vol. 46, No. 19* *Published online 31 July 2018*
doi: 10.1093/nar/gky682

ZBTB24 is a transcriptional regulator that coordinates with DNMT3B to control DNA methylation

Joyce J. Thompson[1], Rupinder Kaur[1], Carlos P. Sosa[2], Jeong-Heon Lee[3,4], Katsunobu Kashiwagi[5], Dan Zhou[6] and Keith D. Robertson[1,4,*]

[1]Department of Molecular Pharmacology and Experimental Therapeutics, Mayo Clinic, 200 First Street SW, Stabile 12-58, Rochester, MN 55905, USA, [2]Clinical Genome Sequencing Laboratory, Department of Laboratory Medicine and Pathology, Mayo Clinic, 200 First Street SW, Stabile12-58, Rochester, MN 55905, USA, [3]Department of Biochemistry and Molecular Biology, Mayo Clinic, Rochester, MN 55905, USA, [4]Epigenomics Translational Program, Mayo Clinic, Rochester, MN 55905, USA, [5]Department of Physiology II, Nara Medical University, Kashihara, Nara 634-8521, Japan and [6]Institutes of Biomedical Sciences, Shanghai Medical College, Fudan University, Shanghai, China

Received March 28, 2018; Revised June 29, 2018; Editorial Decision July 17, 2018; Accepted July 17, 2018

ABSTRACT

The interplay between transcription factors and epigenetic writers like the DNA methyltransferases (DNMTs), and the role of this interplay in gene expression, is being increasingly appreciated. ZBTB24, a poorly characterized zinc-finger protein, or the *de novo* methyltransferase DNMT3B, when mutated, cause Immunodeficiency, Centromere Instability, and Facial anomalies (ICF) syndrome, suggesting an underlying mechanistic link. Chromatin immunoprecipitation coupled with loss-of-function approaches in model systems revealed common loci bound by ZBTB24 and DNMT3B, where they function to regulate gene body methylation. Genes coordinately regulated by ZBTB24 and DNMT3B are enriched for molecular mechanisms essential for cellular homeostasis, highlighting the importance of the ZBTB24-DNMT3B interplay in maintaining epigenetic patterns required for normal cellular function. We identify a ZBTB24 DNA binding motif, which is contained within the promoters of most of its transcriptional targets, including CDCA7, AXIN2, and OSTC. Direct binding of ZBTB24 at the promoters of these genes targets them for transcriptional activation. ZBTB24 binding at the promoters of RNF169 and CAMKMT, however, targets them for transcriptional repression. The involvement of ZBTB24 targets in diverse cellular programs, including the VDR/RXR and interferon regulatory pathways, suggest that ZBTB24's role as a transcriptional regulator is not restricted to immune cells.

INTRODUCTION

DNA methylation (5mC), an epigenetic modification occurring at the 5-position of cytosine catalyzed by members of the DNA methyltransferase (DNMT) family, plays a pivotal role in regulating molecular processes and cellular functions, largely through its influence on gene regulation. The DNMT family is comprised of three catalytically active enzymes-DNMT1, DNMT3A, DNMT3B, and the catalytically inactive DNMT3L. DNMT1, the maintenance methyltransferase, preferentially recognizes hemimethylated DNA and is recruited to the replication fork by UHRF1, where it functions to propagate 5mC patterns during cell division (1). The *de novo* DNA methyltransferases, DNMT3A and DNMT3B, through their ability to write new 5mC patterns using DNMT3L as a co-factor, influence embryonic development and drive cellular differentiation (2,3).

Although the DNMTs share some degree of structural homology and overlapping functional targets, the three active enzymes also exhibit significant non-redundancy in terms of their preferred genomic target sites, as highlighted by several selective overexpression and loss-of-function studies (4–7). This specificity for targeting at preferred sites is achieved by a combination of non-overlapping interactions with sequence-specific DNA binding factors, and interactions with specific histone tail post-translational modifications. For example, DNMT3B is recruited by the transcription factor E2F6 to mediate silencing of the germ-line genes, *Slc25a31*, *Syce1*, *Tex11* and *Ddx4* (8). DNMT3B coordinates with components of the polycomb complex to mediate promoter hypermethylation and thereby repression of their common target loci (9). DNMT3B is also selectively recruited to gene bodies of actively transcribed genes via interactions with histone H3 lysine 36 trimethylation

*To whom correspondence should be addressed. Tel: +1 507 266 4886; Email: robertson.keith@mayo.edu

(H3K36me3), where it functions to methylate exons and direct alternative splicing, and methylate alternative start sites to suppress spurious initiation of transcription (5,10). Genetic ablation of *Dnmt3b* in mouse models, or naturally occurring human *DNMT3B* mutations, give rise to aberrantly spliced transcripts, supporting a crucial role for DNMT3B in regulating RNA splicing (11,12). In humans, mutations in *DNMT3B* that typically result in a hypomorphic enzyme, cause the Immunodeficiency, Centromeric instability and Facial anomalies (ICF) syndrome (13).

ICF syndrome is characterized by complete absence or reduced immunoglobulin levels in the presence of normal B-cell counts, centromeric instability on chromosomes 1, 9 and 16 resulting from loss of heterochromatic repeat DNA methylation and heterochromatin, and varying degrees of neurologic defects and facial anomalies (14,15). ICF syndrome is largely regarded as an epigenetic disorder due to the association of DNMT3B with the syndrome. As an increasing number of ICF cases have been characterized, mutations in additional poorly characterized genes have been identified as causative to the syndrome. While patients with mutations in *DNMT3B* are sub-classified as ICF1 (∼50% of ICF cases), mutations in the *ZBTB24* gene result in ICF2 (∼30% of cases) (16). Patients with mutations in the myc-interacting CXXC-zinc finger (*CDCA7*) gene, and an ATP-dependent chromatin remodeling enzyme *HELLS*, result in ICF3 and ICF4, respectively. An additional class, ICFX, comprises cases wherein the underlying mutation remains unidentified (16).

While the function of ZBTB24 remains largely elusive, it is a member of the BTB-POZ family of zinc-finger proteins, currently composed of 49 structurally homologous members mostly implicated in B-cell and T-cell function, primarily through transcriptional repression. All ZBTB family members possess an N-terminal BTB (Broad complex, Tramtrack, and Bric-a`-brac) domain, which mediates homo- or hetero-dimerization and interactions with other transcriptional co-regulators, (*e.g.* N-CoR, SMRT, HDACs, SIN3), a variable number of (C2H2)-type zinc fingers that enable sequence-specific DNA binding, and in some cases an AT-hook domain that mediates non-specific interactions with A-T-rich DNA via the minor groove (17). ZBTB24 is closely related to ZBTB17 (MIZ1, Myc-interacting zinc finger), which activates transcription through interactions with co-activators like p300, or represses expression via interaction with MYC (18–20). Furthermore, MIZ1 forms a ternary complex with DNMT3A and MYC to bring about promoter methylation and repression of MIZ1-specific targets (21), providing one example by which ZBTB family members influence DNA methylation mechanisms. Three ZBTB family members, ZBTB38, ZBTB33, and ZBTB4 bind both unmethylated and methylated DNA, and function as readers of DNA methylation (22). ZBTB24 activates CDCA7 transcription by direct promoter binding (23), but few other targets are known. Additionally, ZBTB24 indirectly repress IRF4 and BLIMP-1, effectively functioning to regulate B-cell proliferation (24). Mechanisms by which ZBTB24 modulates epigenetic marks at its target loci to influence transcription, however, have not been explored.

In the present study, we sought to define ZBTB24's role in transcriptional regulation and determine whether it interfaces in some way with DNMT3B-mediated epigenetic mechanisms. The similarity between the defining phenotypes across ICF subclasses, and the predicted ability of ZBTB24 to bind DNA in a sequence-specific manner, suggested a number of possible mechanisms by which it could interface with 5mC and/or DNMT3B, including acting as a DNMT3B recruitment factor, a 5mC reader, or regulating some of the same pathways as DNMT3B. Using chromatin immunoprecipitation coupled with deep sequencing (ChIP-seq), we mapped genomic sites bound by these two factors and integrated binding patterns with effects on transcription and genome-wide 5mC patterns arising from independent loss of function of the two factors. Integrative analysis of ChIP-seq, RNA-seq, and 5mC, along with other defining chromatin features, allowed us to define independently and coordinately regulated genomic loci and show that co-binding by ZBTB24 and DNMT3B at actively transcribing ICF-relevant genes regulates gene body 5mC levels.

MATERIALS AND METHODS

Molecular cloning and vector information

ZBTB24 isoform 1 (full-length), ZBTB24 isoform 2 (short isoform lacking seven zinc fingers), and DNMT3B1 (24) were cloned into pLVX3-CMV-Puro using EcoRI and XhoI sites. ZBTB24 was also cloned into pCMV-Tag2B, pcDNA4-HisMaxC, and pM using the same restriction sites. The region of ZBTB24 encoding amino acids corresponding to the eight C2H2 zinc finger domain (amino acids 294–512) was PCR amplified and cloned into pGEX-5X-1 using the EcoRI and XhoI sites.

Cell culture

HCT116 parental cells (from the American Type Culture Collection) and the DNMT3B knockout isogenic line (25) were cultured in McCoy's 5A medium supplemented with 10% FBS and 2 mM L-glutamine. HEK293T cells were cultured in DMEM supplemented with 10% FBS. The B-cell lines Reh, 697 and U266 were cultured in RPMI supplemented with 20% FBS.

Lentiviral production and generation of stable lines

Lentiviral production and transduction were performed as described in (26). Detailed procedures are described in the Supplemental Experimental Procedures.

Western blotting

Western blot analysis was performed using a LiCor system according to the manufacturer's protocols. Information on exact conditions and antibodies is listed in the Supplementary Experimental Procedures.

Immunofluorescence assay (IFA) and imaging

For IFA, HCT116 cells were seeded on poly-L-lysine coated coverslips, fixed with 4% paraformaldehyde (Electron Microscopy Sciences, 15710) and permeabilized with 0.25% Triton-X-100. Blocking was performed with 5% bovine

serum albumin for 1 hour in a humidified chamber at 37°C, followed by incubation with primary antibody (FLAG-M2, 1:1000) for 90 min, followed by secondary, TRITC-anti-mouse (1:2000) for 60 min with washes with 0.5% PBST in between. Nuclei were counterstained with Hoechst stain. Images were acquired using the 405 and 561 nm lasers on a confocal microscope (Zeiss LSM 780) using the 63× oil immersion objective at the Mayo Clinic imaging facility. Images were processed using the Zenlite software and are represented in grayscale.

Immunoprecipitations

Co-transfected cells were trypsinized, washed with ice cold PBS, and lysed in 1× RIPA supplemented with protease inhibitors. Protein content was estimated and 500–800 μg of protein was diluted with 1× PBS and used for each immunoprecipitation reaction. FLAG-IP was performed using washed pre-conjugated anti-FLAG-M2 beads (Sigma), for 4 h at 4°C. Xpress antibody IP was performed by adding washed protein G sepharose beads along with 1 μg anti-Xpress antibody, also for 4 h at 4°C. Washes were performed using 1× PBS and immune complexes were eluted in 1× Laemmli buffer.

Chromatin immunoprecipitation (ChIP), sequencing, peak calling, and downstream analysis

For ChIP, 20 million cells were fixed with 1% formaldehyde, washed with ice cold 1XTBS and lysed in lysis buffer (10 mM Tris–HCl, pH 7.5, 10 mM NaCl, 0.5% IGEPAL). Cells were then subjected to MNase digestion (NEB, M0247S) in digestion buffer (20 mM Tris–HCl, pH 7.5, 15 mM NaCl, 60 mM KCl, 1 mM $CaCl_2$), following which the chromatin was sonicated using a Diagenode Twin sonicator. An aliquot of input chromatin was quantified with a Qubit 3.0 fluorimeter. Anti-FLAG M2 conjugated magnetic beads (Sigma) were added to immunoprecipitate FLAG-only and FLAG-fusion bound regions. After overnight pull-down, beads were washed with ChIP buffer, high salt, low salt, Tris–LiCl and Tris–EDTA buffers followed by elution and reverse cross-linking. DNA was treated with RNAse and extracted with proteinase K followed by purification with the Qiagen MinElute kit. Purified DNA was size selected and sequencing libraries were prepared. Paired-end sequencing was run on the Illumina HiSeq2000 platform at the Mayo Clinic Medical Genome Facility.

Sequencing reads were mapped to the hg19 genome using Burrows-Wheeler alignment (BWA) (27), then peaks were called using the -callpeak function in MACS2 (28). Corresponding inputs served as controls. Peaks occurring in the FLAG-only background were filtered out from the FLAG-ZBTB24 and FLAG-DNMT3B ChIP-seq datasets. Common overlapping peaks were identified using the BEDtool suite's closest function, and peaks were merged using the merge function to give the final dataset for each factor. Peaks were annotated using the annotatePeaks function in HOMER (Hypergeometric Optimization of Motif EnRichment) and recognition motifs were identified using the MEME-suite (29) and the findMotifsGenome function in HOMER. ChIP-seq data representation was performed using modified scripts from deepTools (30).

RNA extraction and expression analysis by qRT-PCR and RNA-seq

RNA was extracted using the Trizol method followed by DNAse treatment. Two micrograms of RNA was subjected to cDNA synthesis using the Superscript II kit. QRT-PCR was performed using BioRad's SsoSyBrGreen. Primer sequences are listed in Supplementary Table S6. Stranded RNA-seq was performed at the University of Minnesota Genomics Center. Libraries were prepared using the TrueSeq kit and paired-end sequencing was performed on a HiSeq2500. Resulting reads were processed using the New Tuxedo Suite (31) and CuffDiff was used to detect differential expression.

Genomic DNA extraction, IlluminaMethylation BeadChip EPIC (850k) array, and downstream DNA methylation analysis

Genomic DNA was extracted by proteinase K digestion followed by phenol:chloroform extraction. DNA concentration was estimated using PicoGreen and 500 ng was bisulfite treated and analyzed on the IlluminaMethylation BeadChip EPIC array (850K). Downstream processing was performed using the R bioconductor package 'minfi'. Probes with a detection P-value <0.05 were removed from further analysis. Methylation changes post-ZBTB24 knockdown were estimated by comparing beta values in the shZBTB24 samples to the shNT control samples, and a change of $|\Delta\beta| > 0.08$ was considered to be significantly differentially methylated. Differential methylation in the HCT116 DNMT3BKO system was determined by comparison with the HCT116 parental cells, and a threshold of $|\Delta\beta| > 0.2$ was used to define significantly differentially methylated probes. Probes were annotated using defined annotations provided by Illumina. Data representation was performed using packages in R.

Recombinant GST protein production and purification

The ZBTB24 zinc finger region-GST construct was transformed into BL21(DE3) competent cells. A single colony was cultured overnight at 37°C in 5 ml of LB-ampicillin (100 μg/ml). 500 μl of the pre-culture was then added to 500 ml of LB-ampicillin broth supplemented with 1 mM $ZnCl_2$ and cultured at 37°C, 200 rpm. Once the OD_{600} reached 0.6–0.8 absorbance units, IPTG was added to a final concentration of 0.1 mM and induction was continued for 4 hours. Bacterial cells were pelleted at 8000 rpm and washed with ice cold PBS-20% glycerol. The pellet was resuspended in 30 ml sonication buffer (20 mM Tris–HCl pH 7.5, 100 mM NaCl, 0.1% deoxycholic acid, 100 mM $ZnCl_2$, 1 mM DTT, protease inhibitors), and sonicated on ice using a Branson soniocator at 50% power and an output of 45 for 5 cycles (10 s on/ 1 min off). Bacterial debris was pelleted at 10 000 rpm for 10 min, and the supernatant was incubated with 300 μl of pre-washed gluththione-sepharose resin for 6 h at 4°C. Bound protein was washed with wash buffer (200

mM Tris–HCl pH 7.5, 100 mM NaCl, 0.1% deoxycholic acid, 100 mM $ZnCl_2$, 1 mM DTT). Protein was eluted with freshly prepared elution buffer (50 mM Tris pH 8.0, 10 mM reduced glutathione). Integrity of the purified protein was monitored by SDS-PAGE gel and staining with Commassie Brilliant Blue.

Electrophoretic mobility shift assay (EMSA)

EMSA conditions were adapted from (32) and EMSA was performed using double-stranded DNA oligonucleotides labelled with IR700 (top strand only) designed based on promoter sequences containing the ZBTB24 motif and bound by ZBTB24. Purified recombinant protein was incubated with labelled oligonucleotides in binding buffer (8 mM HEPES pH 7.9, 80 μM EDTA, 50 mM KCl, 8% glycerol, 40 μg/mL BSA, 10 μM $ZnCl_2$, 10 μg/ml poly(dI-dC), and 0.2 mM DTT) for 30 min in the dark, at room temperature. Samples were then resolved on a 5% non-denaturing PAGE gel in 1× TBE run at a constant voltage of 100 V for 1.5 h. In-gel detection was performed using the LiCor system using the manufacturer's protocol. For qualitative competition assays, unlabeled double stranded probes were used in increasing concentrations in identical conditions as described above.

Luciferase assay

HEK293T cells were co-transfected with the indicated ZBTB24 constructs and pG5-luc or pZBTB24 Motif-luc. Forty-eight hours after transfection, cells were lysed using the Promega-Dual-Luciferase Reporter Assay System Kit (E1960) and luciferase activity was measured using a 'Fluostar Omega' plate reader, using the manufacturers' recommended protocol. A more detailed description is provided under the Supplemental Experimental Procedures.

ENCODE datasets

Raw bam files corresponding to HCT116-specific chromatin marks mapped by ChIP-seq were downloaded from the ENCODE data base. Samples used in our analysis are listed in Supplementary Table S2.

RESULTS

ZBTB24 is a ubiquitously expressed nuclear protein

Since one of the defining features of ICF syndrome is an immunological defect, we postulated that ZBTB24 is selectively expressed in immune cells, along with DNMT3B, CDCA7, and HELLS. Quantitative RT-PCR analysis across a panel of normal human tissues and cancer cell-lines of diverse cellular origin, however, show that ZBTB24 is ubiquitously expressed (Supplementary Figure S1A–C), an observation supported by previous findings from De-Greef *et al*. (33). The other three ICF factors are also ubiquitously expressed (Supplementary Figure S1A–C). RNA-seq counts from a diverse group of cell lines and tissues also show that ZBTB24 expression is not restricted to cells or tissues of immune origin (Supplementary Figure S1D–E). This led us to further question whether ZBTB24 participated more broadly in molecular mechanisms central to cellular or organismal homeostasis. To decipher ZBTB24-regulated mechanisms and identify its targets throughout the genome, we turned to the well characterized colorectal cancer cell line HCT116 as our model system to characterize ZBTB24, and determine whether a functional interplay exists between DNMT3B and ZBTB24.

Due to the lack of a suitable ChIP-seq-compatible ZBTB24 antibody, we created stable cell lines ectopically expressing FLAG-tagged ZBTB24. FLAG-ZBTB24 was introduced into cells via lentiviral-mediated transduction, after which cells were subjected to puromycin selection and single-cell colonies isolated by limiting dilution. Colonies were screened by western blot and immunofluorescence, and three independent clones were selected for further study. Western blotting of the three clones shows expression of FLAG-ZBTB24 at levels similar to endogenous ZBTB24 (Figure 1A and Supplementary Figure S2A–B). FLAG-ZBTB24 in all three clones localizes exclusively to the nucleus, which is demarcated by Hoechst staining, and forms punctate foci (Figure 1B and Supplementary Figure S2C) typical of transcription factors and other nuclear factors (34). To identify ZBTB24 transcriptional targets, we mapped its binding sites across the HCT116 genome by ChIP-seq.

ZBTB24 is enriched at active promoters and enhancers

The three clones expressing FLAG-ZBTB24 were independently subjected to ChIP using anti-FLAG-M2 beads, followed by next-generation sequencing. Inputs for each of the clones were also sequenced, and served as normalization controls during peak calling. We also generated and isolated two single cell HCT116 clones expressing the FLAG-tag only, and along with their corresponding inputs, subjected them to ChIP-seq to identify genomic loci bound non-specifically by the FLAG-tag only. These peaks were deemed noise or FLAG-only background, and removed from peaks identified in FLAG-ZBTB24 expressing clones. As shown in Figure 1C, the three HCT116 FLAG-ZBTB24 clones show a high degree of correlation for ZBTB24 binding. Through comparative analysis between the three clones, we selected peaks that overlapped between at least two of the three clones, and merged the resulting peaks to give a final list of 6173 genomic loci bound by ZBTB24 (Supplementary Table S1). Supplementary Table S2 lists details from the sequencing and mapping and Supplementary Table S3 lists the number of peaks called by MACS2 for each of the clones subjected to ChIP-seq, and the total number of peaks before and after noise (FLAG background) correction.

To identify genomic features bound by ZBTB24, ChIP-seq peaks were annotated to the hg19 genome using HOMER. As indicated in Figure 1D–E, ZBTB24 is enriched upstream of the transcription start site (TSS) of genes, specifically at promoters with high CpG content (full list of promoters provided in Supplementary Table S4). ZBTB24 is also enriched in regions encoding certain classes of non-coding RNA genes. To define the histone marks that co-localize with ZBTB24 binding, we used the HCT116-specific histone modifications from the ENCODE database (Figure 1F and Supplementary Table S5) and cen-

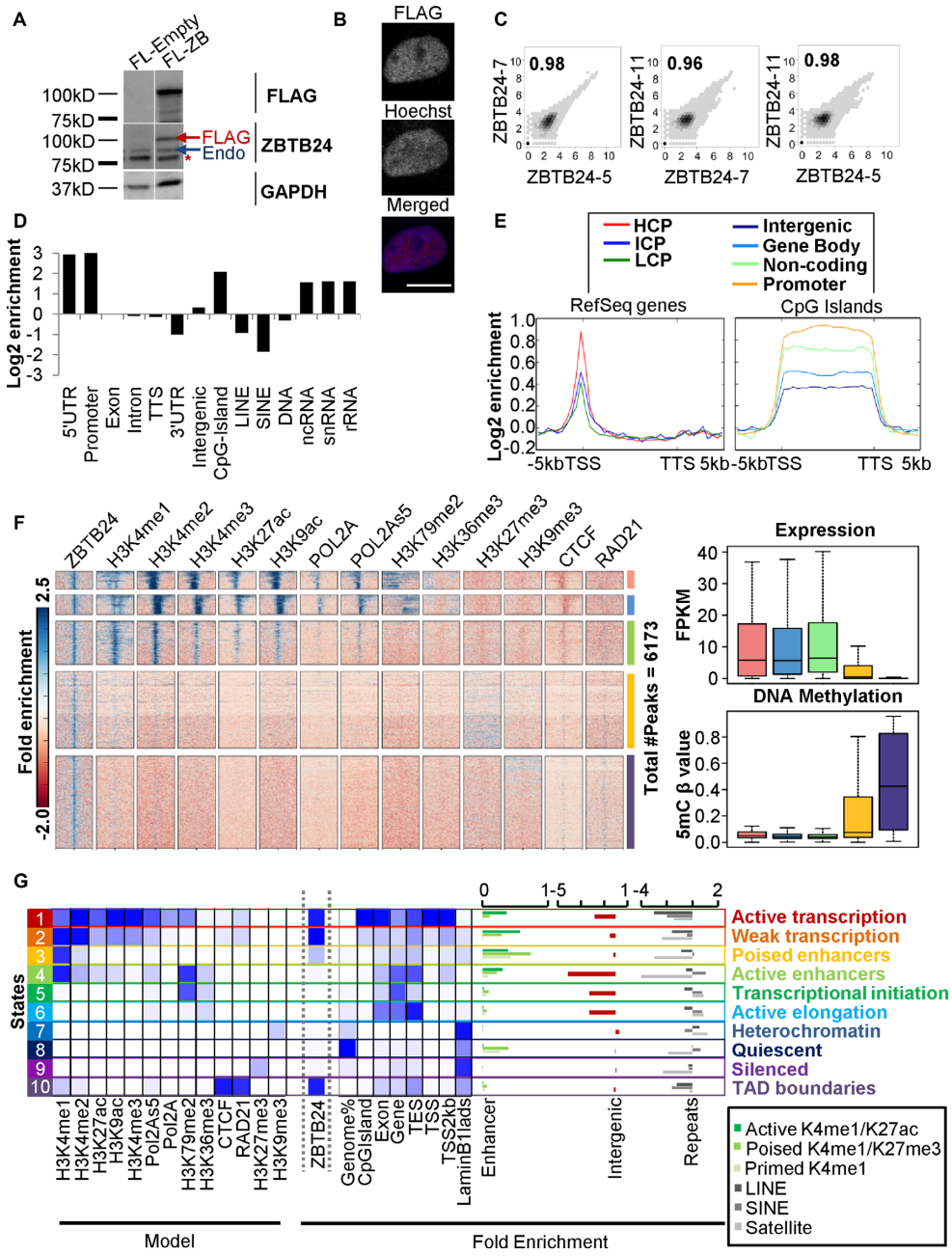

Figure 1. Genome-wide binding properties of ZBTB24. (**A**) Western blot of a representative single cell clone of HCT116 ectopically expressing FLAG-ZBTB24 (FL-ZB). The migration of endogenous ('Endo') and ectopic ZBTB24 ('FLAG') is noted. The antibody recognizes a non-specific band (denoted by *) just below the band corresponding to endogenous ZBTB24. (**B**) Representative immunofluorescence microscopy image showing that FLAG-ZBTB24 localizes to the nucleus, defined by Hoechst staining, and forms punctate foci typical of transcription factors. Scale bar corresponds to 10 microns. The same HCT116 cell clone is used in parts A and B. (**C**) Three independent single-cell clones (ZBTB24–5, −7 and −11) expressing FLAG-ZBTB24 were used to perform ChIP with anti-FLAG-M2 beads, followed by deep sequencing. Scatterplots show genome-wide correlation of ZBTB24 binding between the independent clones, calculated based on log2-transformed read counts across the entire genome divided into windows of 1kb (number of bins = 1,048,575). The Pearson correlation for each pairwise comparison is shown. (**D**) Enrichment of FLAG-ZBTB24 peaks across different genomic features depicted as log2-fold enrichment. Peaks overlapping between the three independent FLAG-ZBTB24 clones were merged and annotated to the hg19 genome, and enrichment at specific genomic features was calculated using HOMER. (**E**) Average ZBTB24 binding profile across Refseq genes sub-classified based on their CpG content (HCP-high, ICP-intermediate, LCP-low, left panel), and at CpG islands (based on their location relative to genes, right panel), is shown as the log2-fold enrichment over input. (**F**) Heatmap of histone marks specific to HCT116 (obtained from the ENCODE database) centered on ZBTB24 peaks subjected to k-means clustering, divides the 6173 ZBTB24 peaks into five clusters, each co-localizing with a distinct set of histone marks. The average expression and methylation levels of loci within individual clusters are shown as box-plots at the right. The five bars within the boxplots correspond to the heatmap clusters and are depicted as unique, matching colors. Methylation and expression levels were profiled in HCT116 parental cells using the IlluminaMethylation BeadChip EPIC (850k) array and RNA-seq, respectively. (**G**) ChromHMM modeling to define links between ZBTB24-bound loci and genome/epigenome features. The genome is divided into ten states of distinct activity or property based on co-localization of histone marks and the enrichment of ZBTB24 binding within each of these states (depicted as fold enrichment). Enrichment of different classes of enhancer, intergenic, and repetitive elements is illustrated as accompanying bar charts at the right.

tered them on ZBTB24 peaks. K-means clustering groups ZBTB24 target loci into distinct chromatin environments, as shown in the heatmap in Figure 1F (and Supplementary Figure S2D). The relative expression and DNA methylation levels associated with each category is illustrated at the right. DNA methylation and expression levels were profiled in HCT116 parental cells using the IlluminaMethylation BeadChip EPIC (850k) array and RNA-seq, respectively. In Figure 1F, clusters 1 and 2 co-localize with marks of active transcription (based on presence of the active promoter mark, H3K4me3, and the active gene body marks, H3K79me2 and H3K36me3 (35,36)), whereas cluster 3 co-localizes with features characteristic of enhancers (based on presence of the enhancer specific marks—H3K4me1, H3K4me2 and H3K27ac, along with the absence of histone marks characteristic of transcribing gene bodies (35)). These three clusters are associated with low levels of DNA methylation and high expression. To define additional chromatin features underlying ZBTB24-bound loci, we used ChromHMM (36) to divide the genome into ten states with functionally distinct activities. The fold enrichment of ZBTB24 within each of these states was determined. As shown in Figure 1G, ZBTB24 is enriched at states 1, 2 and 3, corresponding to promoters of actively transcribed genes and enhancers. Further classification of promoters into distinct groups based on activity, CpG content, and expression status shows that ZBTB24 preferentially binds H3K4me3-marked promoters of highly transcribed genes with high CpG content (Figure 2A, Supplementary Figure S3A). We also categorized enhancer elements based on their genomic location into promoter-associated, intra- and intergenic, and into active, poised, or repressed based on established definitions (35). As shown in the top- and bottom-most group of panels in Figure 2B and Supplementary Figure S3B, ZBTB24 is enriched at promoter-associated and intergenic enhancers that are either active or primed, and relatively depleted from enhancers associated with gene bodies. Promoters of the *CDCA7* and *OSTC* genes, for example, are highly enriched for ZBTB24 binding (Supplementary Table S4), as reported previously (23). Additionally, ZBTB24 is enriched at the *CDC40* gene, one of its reported transcriptional targets (that was not examined for direct ZBTB24 binding previously (23)). Our study also identifies the promoters of *ARID5B*, a transcriptional cofactor of *SOX9* that drives chondrogenesis (37) and polymorphisms in which are associated with risk for lymphoblastic leukemia (38–40), *HOXB7*, an established master regulator of proliferation and osteogenesis (41), *RNF169*, an E3 ubiquitin ligase negatively regulating the ubiquitin-mediated DNA double-strand break response involving 53BP1 (42), *CAMKMT*, a lysine methyltransferase regulating calmodulin and calcium-mediated cell signaling (43), and *AXIN2*, a mediator of the TGFβ pathway involved in directing diverse developmental programs (44), as ZBTB24 targets. A complete list of ZBTB24 target promoters is provided in Supplementary Table S4. Ingenuity Pathway Analysis (IPA) for genes with ZBTB24 bound at their promoter shows enrichment for functions in diverse cellular pathways, like amino acid metabolism, oxidative stress response, telomere function, apoptosis, and differentiation (Supplementary Figure S3C), suggesting ZBTB24 functions are not restricted to immune cell-related processes.

A subset of ZBTB24 peaks co-localize with repressive chromatin domains

While the majority of ZBTB24 peaks co-localize with active histone marks, a subset co-localize with repressive H3K27me3- and H3K9me3-containing regions, as depicted by the heatmaps in Figure 1F and Supplementary Figure S2D. This observation suggests that ZBTB24 plays a role in organizing and maintaining repressive chromatin domains, which is consistent with another defining phenotype of ICF syndrome patients, loss of H3K9me3-rich pericentromeric heterochromatin organization. The ChromHMM model in Figure 1G also reveals that ZBTB24 is not only enriched at promoters of actively transcribed genes and at poised enhancers, but also co-localizes with CTCF and RAD21 (of the cohesin complex), two factors contributing to the organization and maintenance of boundaries at topologically associated domains (TADs) (45). This association with CTCF and RAD21 is also depicted in the heatmaps in Figure 1F and Supplementary Figure S2D, albeit at a lower intensity compared to its enrichment at promoters.

ZBTB24 recognizes the DNA sequence motif AGGTCCTGGCAG within its target regions

De novo motif discovery by HOMER using all ZBTB24 ChIP-seq peaks identified the sequence AGGTCCTGGCAG as the primary recognition motif (*P*-value 1e-867), occurring in 30.78% of ZBTB24 peaks, and with 72% of the ZBTB24-bound promoters containing this motif (Figure 2C). The ZBTB24 recognition motif occurs in many genomic features, but is most abundant in promoters and intragenic regions like exons (Figure 2D). However, use of ChromHMM reveals that ZBTB24 binding is enriched at its motif only within promoters associated with active histone marks; no enrichment is observed at its motif when associated with repressive histone modifications (Figure 2E), suggesting these marks serve as pre-requisites for ZBTB24 binding at its recognition motif. The putative ZBTB24 binding motif shares similarity to motifs recognized by factors belonging to the nuclear receptor class, specifically ESSRA (estrogen-related receptor alpha, data not shown), suggesting ZBTB24 functions as an intermediate in pathways regulated by nuclear receptors. Although the majority of ZBTB24 peaks contain the AGGTCCTGGCAG motif (with variation in nucleotide composition within the motif indicated by the underlined positions, Figure 2C and Supplementary Figure S3D), a small fraction of ZBTB24 target sites contain motifs for known DNA binding factors (Supplementary Figure S3D), including REST and GATA6, which are central to developmental processes (46–49). Figure 2F–G illustrate representative ZBTB24 peaks and motif positions, along with co-localization of select histone modifications, at the promoters of the *CDCA7* and *CDC40* genes.

To independently confirm the ZBTB24 ChIP-seq binding data and gain additional support that ZBTB24 indeed binds the AGGTCCTGGCAG motif, we used ChIP coupled to quantitative PCR (qPCR) to measure ZBTB24 binding at

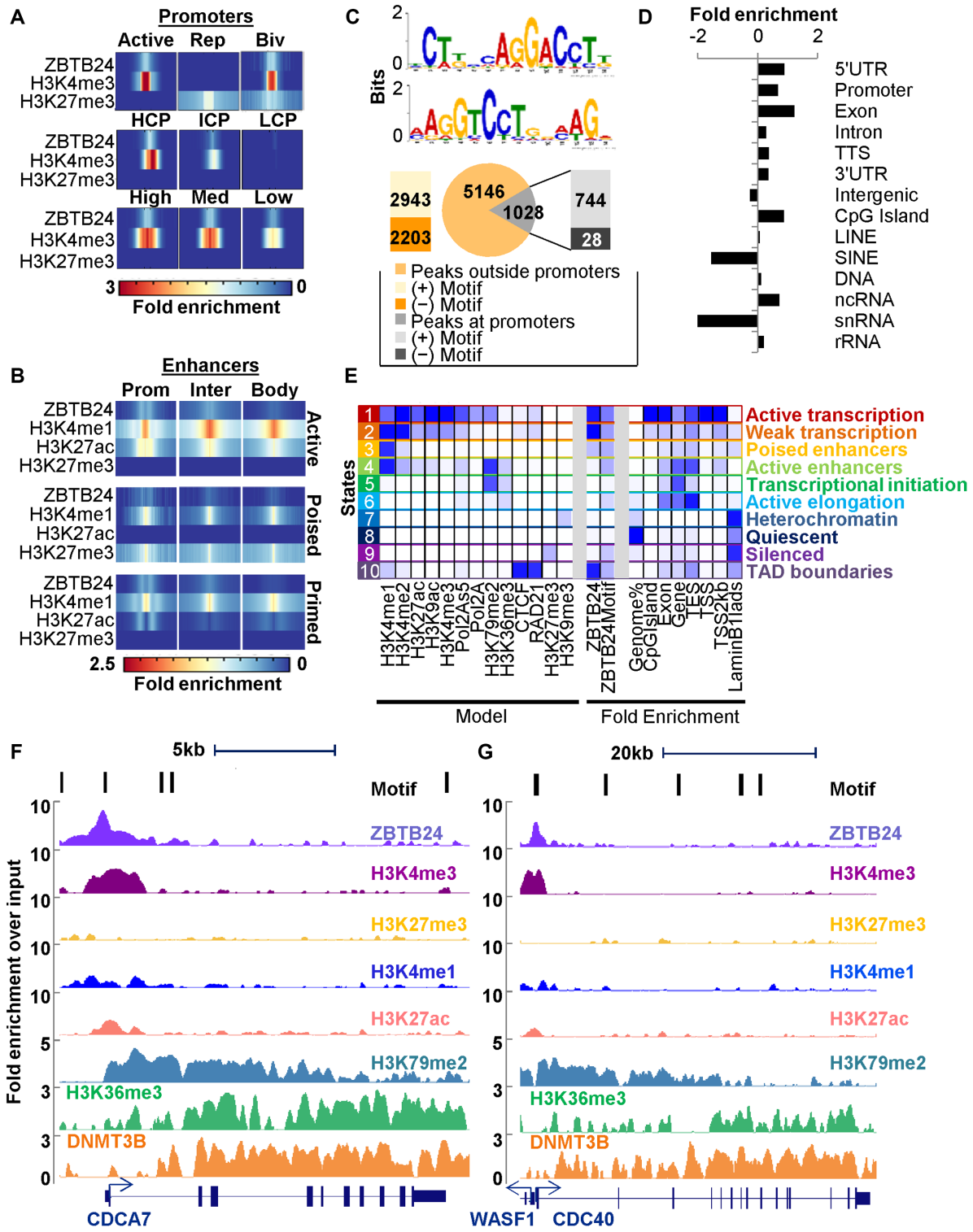

Figure 2. ZBTB24 is preferentially enriched at active promoters and enhancers. (**A**) Average ZBTB24 binding profile at promoters genome-wide, classified based on co-localization with H3K4me3, H3K27me3, and activity status (active, repressed-'Rep', and bivalent-'Biv' domains), CpG content, and expression level (high, medium, low). (**B**) ZBTB24 binding profile at enhancers classified as active, poised, and primed, based on co-localization with H3K4me1, H3K27ac, and H3K27me3, and further sub-classified into promoter (prom), intergenic (inter), and gene body (body), based on the genomic feature they are associated with. (**C**) Putative ZBTB24 DNA recognition motif identified using HOMER based on ChIP-seq. The pie chart shows the distribution of ZBTB24 peaks within and outside promoters, and the adjacent bar charts show number of peaks within each category containing the indicated motif. (**D**) Genome-wide occurrence of the ZBTB24 DNA binding motif from part C irrespective of ZBTB24 binding defined by ChIP-seq. (**E**) Enrichment of the predicted ZBTB24 recognition motif across different states defined in the ChromHMM model from Figure 1G. ZBTB24 is bound at the predicted motif in states marked by active, but not repressive histone marks. Representative browser views of the *CDCA7* locus (**F**) and the *WASF1*/*CDC40* locus (**G**) with ZBTB24 binding in their promoter regions, as well as tracks for other relevant epigenetic marks.

10 promoter-ZBTB24 target loci (identified by ChIP-seq and containing the top ZBTB24 binding motif discussed above; a subset of those loci are listed in Supplementary Figure S4A and represent the most ZBTB24-enriched promoter loci defined by ChIP-seq) using primers flanking the motif-containing region (Supplementary Figure S4B–C). These 10 loci show robust enrichment of ZBTB24 by ChIP-qPCR relative to HCT116 cells expressing the empty FLAG control and relative to the *GAPDH* promoter that does not contain ZBTB24 peaks or the motif (Supplementary Figure S4C). Promoters of BEND7, APOL1, and MYO6 served as additional negative controls for ZBTB24 binding (Supplementary Figure S4B). These three promoters contain the ZBTB24 motif but were not recovered as ZBTB24 binding targets in ChIP-seq. Additionally, the LIN37 and RDM1 promoters, which were recovered as binding targets in ChIP-seq (but do not contain the high-scoring DNA motif) serve as additional positive controls. As is evident from the ChIP-qPCR in Supplementary Figure S4C, these latter two loci are associated with lower ZBTB24 enrichment as compared to those containing the motif, but show binding above background nonetheless. Since the ICF syndrome is associated with a defect in B-cell function, we examined ZBTB24 binding at its motif-containing regions within these promoters in B-cells. ChIP for endogenous ZBTB24 was performed using three B-cell lines and in parental HCT116 cells without ectopic FLAG-ZBTB24 expression, followed by qPCR at the same regions tested in Supplementary Figure S4B. In general, ZBTB24 targets identified by FLAG-ChIP-seq in HCT116 cells are also positive for endogenous ZBTB24 binding across the three B cell lines and parental HCT116 cells (Supplementary Figure S4C–D). Overall this data shows that ZBTB24 binding targets identified by FLAG ChIP-seq are conserved across cell types, suggestive of a functional role of ZBTB24 not restricted to immune cells.

We further validated the ZBTB24 motif using electrophoretic mobility shift assays (EMSA). The yield and purity of full-length ZBTB24 was poor as a GST-fusion protein in *Escherichia coli* (not shown), therefore we expressed and purified a region of the protein corresponding to its eight zinc-fingers (a.a 294–512). Supplementary Figure S4E shows the purity of the recombinant ZBTB24 zinc finger domain. Using promoter regions from three ZBTB24 target genes, CAMKMT, OSTC and CDCA7, we designed IR700 labelled oligonucleotides containing the motif. The GAPDH promoter, and a region of the CDCA7 promoter distant from the ZBTB24 motif region, served as negative controls. As shown in Figure 3A and the top two panels of Supplementary Figure S4F, incubation with increasing amounts of the purified GST-ZBTB24 zinc finger domain shifted the free probe, indicating binding by the recombinant protein. No shift was observed with the GAPDH and CDCA7 promoter sequences not containing the ZBTB24 motif (Supplementary Figure S4F, bottom two panels). We also performed competition assays with unlabeled wild-type and mutant probes corresponding to the oligonucleotides designed using the CAMKMT promoter (Figure 3B). Increasing concentration of the unlabelled wild-type, but not the mutant probes effectively reduced binding of the ZBTB24 zinc finger domain to the labeled oligonucleotides (Figure 3C) demonstrating that the zinc-finger region recognizes the motif overrepresented in our ZBTB24 ChIP-seq peaks.

To examine the ability of the identified ZBTB24 binding motif to modulate expression in a ZBTB24-dependent manner, we cloned it upstream of the luciferase gene (as five copies in tandem) and tested the ability of ectopically expressed ZBTB24 to modulate luciferase activity in HEK293T cells. The ZBTB24 DNA motif-containing luciferase vector was co-transfected with increasing amounts of a control empty expression plasmid (used to normalize for transfection efficiency and plasmid DNA content), or increasing amounts of a full-length wild-type form of ZBTB24 (ZB-L, Supplementary Figure S4G) containing all eight zinc fingers. A naturally occurring splice variant of ZBTB24 (ZB-S, Genbank KJ892863.1, Supplementary Figure S4G), which lacks all but one of the zinc fingers, is used as a reference since it is predicted to lack DNA binding activity. As shown in Supplementary Figure S4H, full-length ZBTB24 robustly induces reporter gene activity, but the shorter isoform lacking seven fingers shows reduced activation, indicating that ZBTB24 is capable of binding the AGGTCCTGGCAG motif to activate transcription, and that the zinc fingers are critical for this activity.

ZBTB24 activates and represses transcription

To determine the effect of ZBTB24 binding on its target loci in cells, we employed a loss-of-function approach and studied the downstream effect of shRNA-mediated ZBTB24 depletion on gene expression in HCT116 cells using RNA-seq. ZBTB24 is effectively depleted in HCT116 cells at the RNA level and even more so at the protein level (Figure 4A). Cells transduced with a non-targeting shRNA (shNT), served as control. Both shNT and shZBTB24 transfected cells were subjected to RNA-seq in triplicate. Genes showing a 1.5-fold or greater change at *P*-value <0.05 were considered to be differentially regulated upon knockdown of ZBTB24. Comparable numbers of genes are up- and down-regulated after ZBTB24 knockdown, as summarized in the volcano plot in Figure 4B, suggesting ZBTB24 functions as both a transcriptional activator and a repressor, depending on context. To identify direct versus indirect ZBTB24 transcriptional targets, we mapped ZBTB24 binding within promoters or gene bodies of the differentially regulated genes (Figure 4C–D). One hundred forty six of the 1091 up-regulated genes (hypergeometric probability *P*-value 1.51e–44) and 162 out of the 852 down-regulated genes (hypergeometric probability *P*-value 1.41e–44) are bound by ZBTB24 (Figure 4C). In addition, while a large fraction of deregulated genes contain the predicted ZBTB24 binding motif (1160 out of the 1943 deregulated genes), only a fraction of these show ZBTB24 binding by ChIP-seq, suggesting the involvement of additional factors mediating the function of ZBTB24 or limitations in the ability of ChIP-seq to capture all ZBTB24-bound regions (Figure 4C–D). In addition to regulating genes undergoing active transcription, ZBTB24 also targets silenced regions (states 8 and 9, Figure 4D), and regions coordinated by CTCF and RAD21 (state 10, Figure 4D).

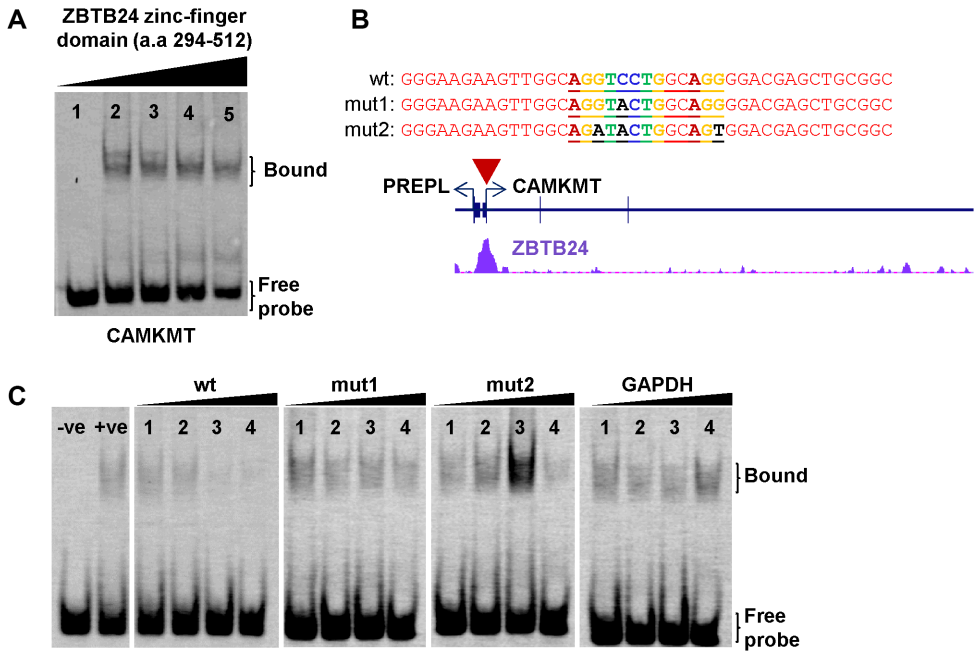

Figure 3. The C2H2 zinc finger region of ZBTB24 recognizes the consensus DNA motif AGGTCCTGGCAG. (**A**) Electrophoretic mobility shift assay (EMSA) performed with recombinant GST-tagged zinc-finger region of ZBTB24 (a.a 294–512) on the consensus DNA motif present within the CAMKMT promoter. Native PAGE gel showing electrophoretic mobility shift of labelled probe upon incubation with increasing amounts of the recombinant protein, indicative of binding. Lane 1 represents the negative control with no recombinant protein added. Lanes 2, 3, 4 and 5 had 4, 8, 16 and 20 μg of recombinant protein added, respectively. (**B**) Position of the ZBTB24 ChIP-seq peak (bottom), EMSA oligonucleotide (red arrowhead) within the CAMKMT promoter, and the sequence of the oligonucleotide (top), both wt and mutant forms, used in the competition assays. The consensus motif is underlined and colors of the bases are adapted from the sequence logo in Figure 2C. Mutations at bases within the motif are indicated in black. (**C**) Competition EMSA performed with varying concentrations of unlabelled wt (second panel) or mutant oligonucleotides (third and fourth panels-mut1/2) in the presence of a fixed amount of wt labelled probe and recombinant protein (4 μg). Competition with unlabelled probe corresponding to the GAPDH promoter serves as a control in the competition assays. Lanes 1, 2, 3 and 4 correspond to addition of unlabelled probe at concentrations of 4×, 10×, 20× and 200× of the labelled probe, respectively. Negative and positive controls for the EMSA itself, were labeled probe with or without recombinant ZBTB24 added respectively, and without addition of unlabeled competitor probe (first panel).

We then examined whether genes showing differential expression upon ZBTB24 depletion showed an inversely regulated pattern of expression in the single-cell clones expressing FLAG-ZBTB24 ectopically (i.e. up-regulation with ZBTB24 knockdown and down-regulation by ZBTB24 ectopic expression or vice versa). Expression patterns of the FLAG-ZBTB24 clones used in ChIP-seq were profiled by RNA-seq, the FLAG-empty clones served as controls. Expression of 350 genes is commonly altered in the ZBTB24 knockdown and the FLAG-ZBTB24 ectopic expression system. Out of these, 144 genes are up-regulated upon ZBTB24 knockdown and down-regulated in the FLAG-ZBTB24 expression system, suggesting these loci are targeted for repression by ZBTB24. On the other hand, 87 genes are down-regulated upon ZBTB24 knockdown and up-regulated in the FLAG-ZBTB24-expressing cells, suggesting ZBTB24 acts as a transcriptional activator at these loci (Figure 4E). Genes differentially regulated in the ZBTB24 knockdown system are enriched for functions related to protein ubiquitination, adipogenesis, interferon signaling, and regulation of cell growth and cell death (Figure 4F). Of particular interest is the involvement of ZBTB24 transcriptional targets in pathways regulated by the vitamin D and retinoid X receptors (VDR/RXR), and the interferon regulatory transcription factor (IRF) family. IPA analysis predicts that the transcription factors IRF3/IRF5/IRF7, which share overlapping and distinct functions in regulating the type I interferon response (50,51), are targeted for activation in the absence of ZBTB24, while TRIM24, a cofactor coordinating with hormone receptors to drive proliferation (52) and negatively regulating the interferon response (53), is predicted to be inhibited (Figure 4G). These findings therefore highlight a potential role for ZBTB24 in regulating the immune response and cell proliferation induced by the action of nuclear hormone receptors. We tested the transcriptional changes induced by ZBTB24 depletion at eight loci directly bound by ZBTB24 at their promoters (Figure 4H and Supplementary Figure S5A, top panel). In addition to CDCA7, a reported target of ZBTB24 (Supplementary Figure S5A), AXIN2, a negative regulator of beta-catenin (44), and OSTC, encoding a subunit of the mammalian oligosaccharyltransferase complex (54), are transcriptionally downregulated upon ZBTB24 depletion, suggesting ZBTB24 binding at the promoters of these genes targets them for transcriptional activation (Figure 4H, top). ZBTB24 long-form, containing all eight zinc-fingers, but not the short-form lacking all but one finger, efficiently rescues knockdown-induced downregulation at these three loci (Figure 4H and Supplementary Figure S5A, bottom panels). This suggests that the C-terminal zinc finger containing region of ZBTB24 is essential for transcriptional activation of its target loci. On the

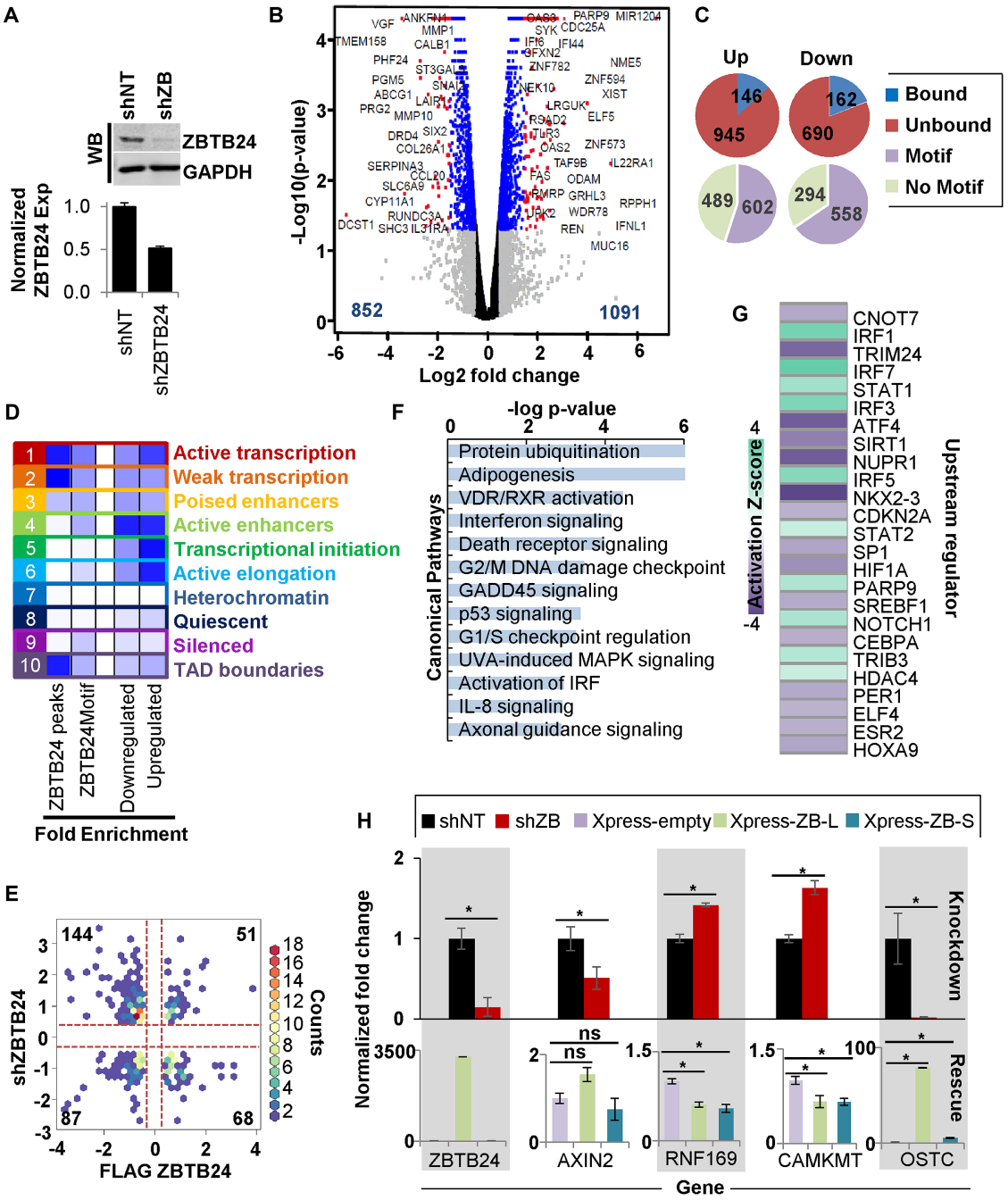

Figure 4. Transcriptional consequences of ZBTB24 binding at its target loci. (**A**) Western blot and qRT-PCR showing the extent of shRNA-mediated acute knockdown of ZBTB24 expression in HCT116 cells. (**B**) Volcano plot of differentially expressed genes upon ZBTB24 knockdown. Genes showing a 0.5 log2-fold change over the non-targeting shRNA control (shNT) at *P*-value <0.05 were considered differentially regulated ZBTB24 targets. (**C**) Fraction of genes transcriptionally regulated and bound by ZBTB24 (by ChIP-seq, upper pie charts) and the fraction of genes containing the predicted ZBTB24 recognition motif (lower pie charts). One hundred forty six out of the total 1091 genes upregulated upon ZBTB24 knockdown contain ZBTB24 peaks (*P* value = 1.51e–44), whereas 602 genes contain the ZBTB24 predicted motif (*P* value = 3.56e–181). In comparison, 162 out of the 852 downregulated genes contain a ZBTB24 peak (*P*-value = 1.41e–71) and 558 genes contain the ZBTB24 recognition motif (*P* value = 2.17e–143). (**D**) Co-enrichment of genes containing the ZBTB24 recognition motif, directly bound by ZBTB24, and up- or down-regulated upon ZBTB24 shRNA knockdown, at each state defined by ChromHMM. ZBTB24 transcriptionally regulates actively transcribed, as well as silenced regions of the genome. (**E**) Inverse correlation between genes differentially expressed upon both ZBTB24 knockdown and ectopic expression of FLAG-ZBTB24 in HCT116 cells. The color scale (counts) depicts number of genes showing the same degree of correlation. (**F**) Molecular pathways regulated by ZBTB24 transcriptional targets. (**G**) Upstream regulators of ZBTB24 transcriptional targets identified by Ingenuity Pathway Analysis. (**H**) Transcriptional changes at select ZBTB24 promoter-bound loci upon knockdown of ZBTB24 (top panel), and the ability of ectopically expressed Xpress-tagged ZBTB24 isoforms to rescue the transcriptional change induced by ZBTB24 shRNA-mediated depletion (bottom panel), assayed by qRT-PCR. Transcript levels are an average of triplicate measures, normalized to transcript levels of the housekeeping gene RPL30, and represented as a fold-change over a control non-targeting shRNA (shNT) or empty Xpress-only control vector transfection in the knockdown and rescue experiments, respectively. Student's t-test is used for statistical comparison and $P < 0.05$ is considered significant and represented with as asterisk; $P > 0.05$ is represented as ns (not significant).

other hand, RNF169, CAMKMT (Figure 4H), and to some extent ZNF451 (Supplementary Figure S5A), are activated upon ZBTB24 depletion, demonstrating that they are targeted for transcriptional repression by ZBTB24 promoter binding. Re-expression of both isoforms of ZBTB24 results in reduced transcript levels of these three loci, suggesting the N-terminal region of ZBTB24 is essential for its repressive function. All genes tested in the rescue studies contained the ZBTB24 recognition motif. The ability of both ZBTB24 isoforms to rescue transcriptional activation of CAMKMT and RNF169 induced by ZBTB24 depletion, suggests that ZBTB24 may be recruited to these promoters via intermediary factors independent of its zinc fingers. ARID5B and CDC40, two of the loci directly bound by ZBTB24 at their promoters, did not show a clear and opposite transcriptional change upon ZBTB24 depletion and re-expression of the two ZBTB24 isoforms, indicating that they are less sensitive to ZBTB24 binding or that other factors compensate in HCT116 cells. Given the interplay between ZBTB24 and CDCA7 shown here and (23), two known ICF genes, we more closely examined whether DNMT3B itself could be a transcriptional target of ZBTB24. As shown in Supplementary Figure S5B, although the DNMT3B promoter contains the active histone mark H3K4me3 in HCT116 cells, it is devoid of a ZBTB24 peak and does not contain the high scoring ZBTB24 DNA binding motif within its promoter (Supplementary Figure S5B). Additionally, ZBTB24 depletion (Supplementary Figure S5C, top panel) does not impact DNMT3B expression (Supplementary Figure S5C, bottom panel), suggesting ZBTB24 does not control DNMT3B expression, at least at the transcriptional level.

We independently examined the transcriptional activity of ZBTB24 by fusing it to the GAL4 DNA binding domain (GAL4-DBD) and co-transfecting it with a luciferase reporter gene driven by five GAL4 DNA binding sites (Supplementary Figure S5D). In this system, GAL4-ZBTB24 robustly induces luciferase activity showing that, at least in this context, it inherently acts as a transcriptional activator. Truncation of the zinc-fingers and the C-terminal region of ZBTB24 in the short isoform, fails to induce reporter activity, suggesting that the C-terminus contributes to the transcriptional activation potential of ZBTB24 since, in this system, it is being recruited to the reporter via the GAL4-DBD rather than its own zinc fingers (Supplementary Figures S4H and S5D).

Loss of ZBTB24 results in genome-wide DNA hypomethylation, preferentially within gene bodies

Since the BTB-POZ family members ZBTB4, ZBTB33, and ZBTB38 bind to or 'read' DNA methylation (55–57), and ICF2 patients with *ZBTB24* mutations display defects in DNA methylation (16), we examined the involvement of ZBTB24 in regulating DNA methylation. We assayed for 5mC changes in HCT116 cells resulting from ZBTB24 depletion, using the Illumina Infinium MethylationEpic BeadChip Array (or '850k' array, interrogating approximately 850,000 CpGs across all human genes and some intragenic regulatory regions). DNA methylation patterns in both control (shNT) and ZBTB24 shRNA knockdown (shZB) cells were profiled in three and two biological replicates, respectively. To detect changes post-ZBTB24 depletion, 5mC levels (detected as beta values-β) at each CpG in each of the knockdown samples were normalized to the levels in shNT control cells (5mC levels at each probe in the control cells were averaged before normalization). The resulting delta beta value (Δβ) represents the degree to which 5mC levels are affected by acute ZBTB24 knockdown. Significant differentially methylated sites are defined as CpGs showing a Δβ greater than 0.08 (hypermethylated) or <0.08 (hypomethylated). A normalized genomic distribution of the resulting 32,827 differentially methylated CpGs (Figure 5A) shows there is an overall trend toward genome-wide hypomethylation in ZBTB24-depleted HCT116 cells. A heatmap of beta values corresponding to differentially methylated CpG sites in the three controls and the two knockdown samples, segregated by their associated genomic feature, shows clear clustering of control and ZBTB24 knockdown conditions (Figure 5B). As shown in the bar chart (Figure 5A), the majority of hypomethylation events are localized to gene bodies (which are typically highly methylated (10,11)), suggesting that the absence of ZBTB24 reduces fidelity and/or recruitment of DNA methyltransferases to these loci. Using DNA immunoprecipitation (DIP) with an antibody specific to 5mC, coupled with qPCR, we confirmed hypomethylation resulting from ZBTB24 depletion at gene bodies, as compared to the 5mC levels in the control cells. (Supplementary Figure S5E). The efficiency of the pulldown of this previously validated antibody (6,58,59) was monitored by using spike-in controls, and is shown in Supplementary Figure S5F.

We next examined relationships between DNA methylation and expression. Since 5mC at promoters and gene bodies has distinct effects on transcription, we segregated genes showing differential methylation after ZBTB24 knockdown by feature, and compared their expression levels (determined by RNA-seq). Figure 5C shows overlap of methylation and expression changes and Figure 5D shows the correlation between promoter and gene-body hyper-/hypomethylation, and gene expression with ZBTB24 depletion. The greatest number of promoter-associated 5mC changes are indeed linked to elevated expression of the associated gene (Figure 5D, upper left quadrant). The general trend toward genomic hypomethylation is also observed in gene bodies, where it correlates comparably with expression changes in both directions, possibly indicating more complex interactions are occurring within bodies, such as intragenic enhancer modulation or changes in DNA hydroxymethylation (which is not detected independent of 5mC with this technique).

To integrate ZBTB24 binding patterns (from ChIP-seq) with effects on DNA methylation and transcription mediated by ZBTB24 shRNA depletion, we made use of ChromHMM. The top-most panel in Figure 5E shows changes in 5mC occurring within each state with ZBTB24 depletion. Changes are depicted as box-plots of Δβ values of significantly differentially methylated CpG sites associated with each state. Similarly, changes in expression resulting from ZBTB24 depletion are presented in the middle panel. The bottom-most ChromHMM panel shows the histone marks co-localizing at each chromatin state and

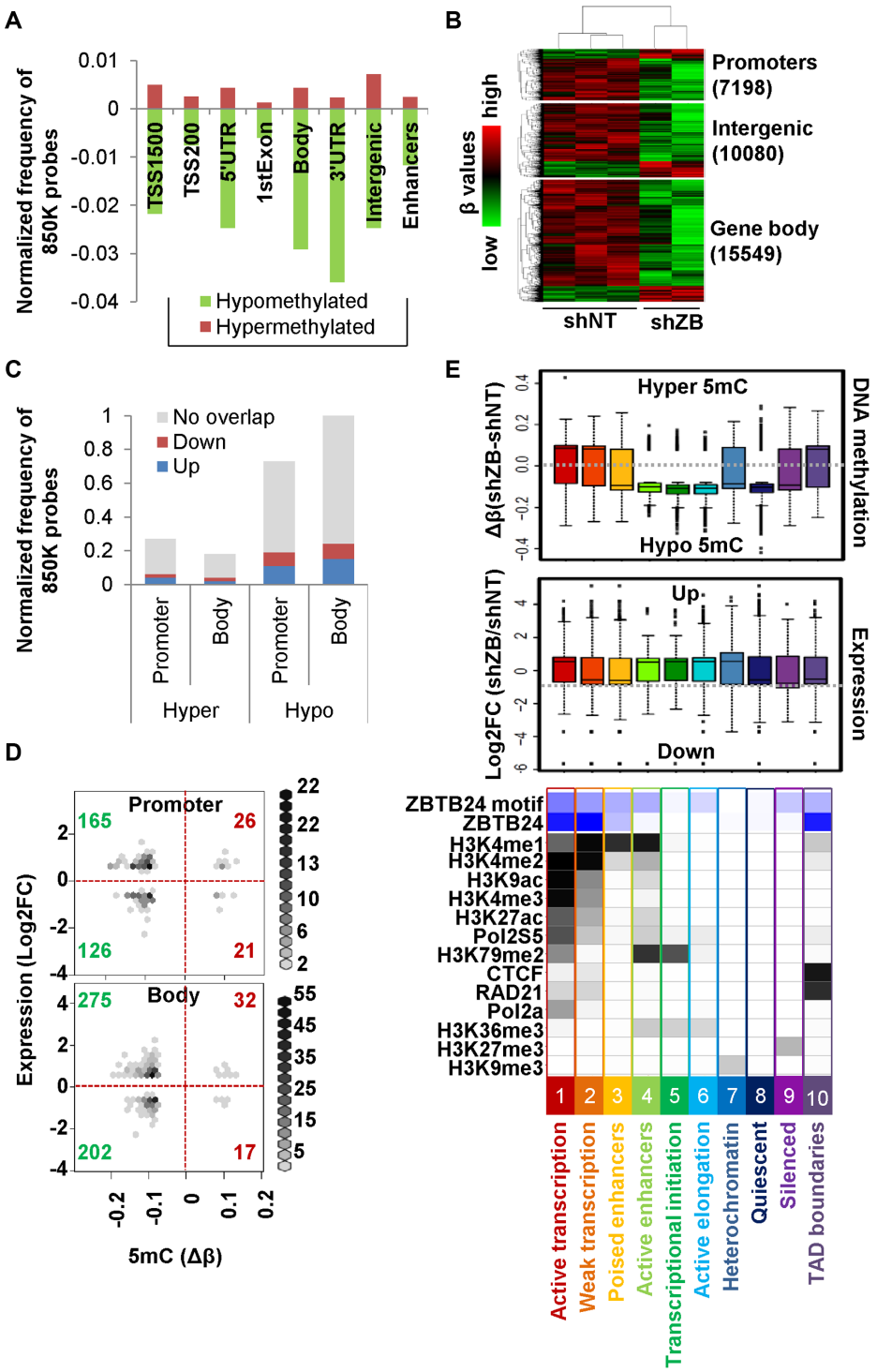

Figure 5. Changes in DNA methylation resulting from ZBTB24 depletion. (**A**) Distribution of DNA methylation changes occurring across genomic features after shRNA-mediated ZBTB24 depletion in HCT116 cells assayed by the Infinium MethylationEpic BeadChip 850k array. Differentially methylated CpGs are defined as sites showing a change ($\Delta\beta$) of $>|0.08|$ compared to shNT cells. (**B**) Heatmap of differentially methylated CpG sites segregated based on their associated genomic feature, shows distinct clustering of the control (shNT) and ZBTB24 knockdown (shZB) replicates. (**C**) Proportion of genes associated with changes in DNA methylation post-ZBTB24 depletion, also showing changes in expression, represented as stacked bar charts. Genes sustaining changes in DNA methylation and upregulation upon ZBTB24 depletion are depicted in blue, whereas genes undergoing changes in DNA methylation and downregulation are depicted in red. (**D**) Hexbin plots illustrating the association between genes undergoing changes in DNA methylation ($\Delta\beta$ cut-off = 0.08) at their promoters (top panel) or bodies (bottom panel), and their corresponding change in expression (log2-fold change cut-off = |0.5|) upon ZBTB24 knockdown. Number of genes in each quadrant is indicated. (**E**) Changes in DNA methylation and expression resulting from ZBTB24 depletion within each chromatin state defined by ChromHMM. The top-most panel shows differential methylation ($\Delta\beta$ cut-off = 0.08) in HCT116 cells upon ZBTB24 knockdown. The middle panel shows differential expression (log2-fold change cut-off = 0.5) upon ZBTB24 depletion. Colors of each bar correspond to the chromatin states in the bottom panel labeled below.

ZBTB24 binding by ChIP-seq within each state. State 1, which corresponds to actively transcribed regions, is enriched for ZBTB24 binding and associated with low 5mC and high transcription. Upon ZBTB24 knockdown, loci within this state gain DNA methylation (red bar in upper boxplot in Figure 5E) and expression (red bar, middle panel), and may therefore represent direct ZBTB24 genomic targets. Since this state includes both promoter elements and 5′-ends of gene bodies (refer to Figure 1G for entire model), the correlation between methylation and expression may be most representative of changes occurring at gene bodies. States 5 and 6, which represent the 5′-end of actively transcribed genes (defined by the presence of H3K79me2 (60,61)) and the 3′-end of gene bodies (defined by presence of H3K36me3/absence of H3K79me2 (60,61)), respectively, are also associated with reduced 5mC and increased transcription. Intragenic DNA methylation, as reported previously, serves to represses spurious initiation of transcription from alternative intragenic promoters (11). Thus, our observation of intragenic hypomethylation and increased transcription in states 5 and 6 could represent increased spurious transcriptional events occurring in the absence of ZBTB24. Heterochromatic and silenced regions of the genome, represented in states 7 and 9, are associated with high levels of 5mC, which are reduced upon ZBTB24 knockdown, suggesting it plays a role in general maintenance of the epigenome at these loci.

ZBTB24 and DNMT3B co-localize at different features of the same gene and function to maintain intragenic DNA methylation

Motivated by the observed genomic hypomethylation upon ZBTB24 depletion, and by the similarity between the phenotypes of ICF1 and ICF2 patients in terms of the 5mC defect, we examined whether ZBTB24 coordinated with DNMT3B in maintaining DNA methylation at its target loci. We first questioned whether the two factors shared genomic targets. Although we have previously used ChIP-seq to map DNMT3B largely to actively transcribed gene bodies (5), DNMT3B localization is not available in HCT116 cells. We therefore mapped DNMT3B binding in HCT116 cells using the same system used to map ZBTB24 (Supplementary Figure S6A–C). Consistent with previous findings (5,10), stable FLAG-DNMT3B1 expressing HCT116 cells showed that DNMT3B is preferentially enriched at gene bodies and is highly co-localized with H3K36me3 (Figure 6A–B, Supplementary Figure S6D–F), a marker of transcriptional elongation (62,63). Due to the preference for ZBTB24 to bind near the TSS, and for DNMT3B to bind within gene bodies, it was not surprising that there were few regions where the two factors co-localized. While ZBTB24 and DNMT3B did not co-bind the same feature, we did observe an association of binding of the two factors. As shown in Figure 6C, ZBTB24 is enriched at a subset of DNMT3B peaks representing exons near to the 5′-ends of genes, suggesting co-binding by both factors at the gene level (Figure 6D). A total of 653 genes show ZBTB24 and DNMT3B co-binding at their promoters and gene bodies, respectively (Figure 6D-E), and functions of their associated gene products are enriched for cellular maintenance, DNA repair, and telomere function (Figure 6F). To identify the functional implication of gene level co-binding, we compared RNA-seq and 850k 5mC data derived from the shRNA depletion studies for ZBTB24 effects, and an isogenic DNMT3B knockout (KO) version of HCT116 cells (25) for DNMT3B effects. The impact of DNMT3B knockout on global DNA methylation and expression, relative to parental HCT116 cells, is summarized in Supplementary Figure S6G–H. Co-bound genes are associated with a modest overall activation of transcription with ZBTB24 depletion, and an average decrease in expression with DNMT3B depletion (from the DNMT3BKO system, Figure 6G). These genes are associated with an average loss of 5mC at both promoters and gene bodies upon ZBTB24 depletion, whereas they show an average gain in 5mC with DNMT3B loss (Figure 6H). The modest gain in 5mC in DNMT3BKO HCT116 cells is consistent with a previous report from our laboratory performed using siRNA knockdown of DNMT3B in NCCIT cells, and is likely due to elevated DNMT1 recruitment at sites previously occupied by DNMT3B (6). The 653 co-bound genes are divided equally into groups based on functional directionality for both expression and methylation (data not shown). This suggests the involvement of additional co-repressor or co-activator complexes involved in mediating the transcriptional outcome of ZBTB24-DNMT3B interaction at co-bound genes. The common outcome of an absence of ZBTB24 or DNMT3B, however, is deregulated DNA methylation within the bodies of co-bound genes, which show the highest degree of correlation (Pearson's correlation coefficient of 0.55 between body 5mC (shZB) and body 5mC (3BKO), Figure 6I), irrespective of the downstream consequence on transcription. This implicates the combined activities of ZBTB24 and DNMT3B as being essential for mediating proper DNA methylation within the bodies of co-bound genes. Co-immunoprecipitation reactions in HEK293T cells demonstrate that ZBTB24 and DNMT3B (but not DNMT1/DNMT3A, Supplementary Figure S6I) interact, suggesting that regulation of the co-bound genes results from interaction between the factors or that ZBTB24 participates in loading DNMT3B onto select gene bodies. We tested the latter idea by performing ChIP with FLAG antibody, coupled with qPCR after depleting endogenous ZBTB24 in one of the FLAG-DNMT3B expression lines used previously in ChIP-seq. The western blot in Supplementary Figure S6J shows effective depletion of ZBTB24 in the FLAG-DNMT3B-expressing HCT116 clone. As compared to control cells, shRNA mediated ZBTB24 depletion results in a modest reduction of DNMT3B occupancy within gene bodies of a subset of the commonly bound genes (Supplementary Figure S6K). We also created HCT116 DNMT3BKO lines stably expressing FLAG-ZBTB24 or FLAG-only (Supplementary Figure S6L). As shown in Supplementary Figure S6M, ZBTB24 remains bound at its target promoters even in the absence of DNMT3B. This data suggests that ZBTB24 participates in recruitement of DNMT3B to gene bodies of their commonly bound loci.

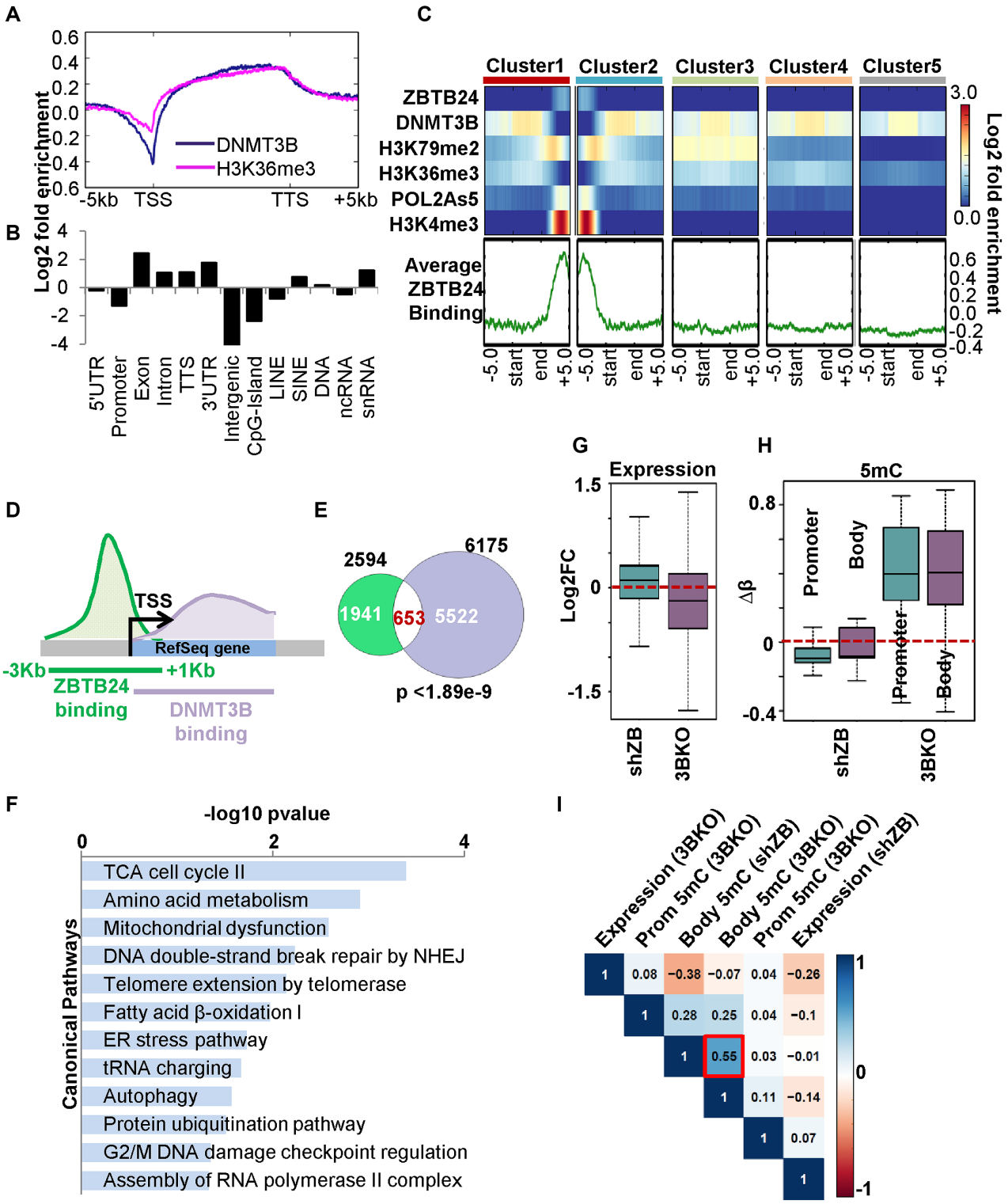

Figure 6. ZBTB24 coordinates with DNMT3B to regulate gene body methylation. (**A**) Average DNMT3B and H3K36me3 binding profile across Refseq genes shown as the log2-fold enrichment over input in HCT116 cells. (**B**) Enrichment of FLAG-DNMT3B merged peaks across different genomic features of the hg19 genome calculated by HOMER and represented as log2-fold enrichment. (**C**) Average ZBTB24 binding profile plotted 5 kb upstream (+5.0) and downstream (-5.0) of FLAG-DNMT3B ChIP-seq peaks, depicted as a heatmap (top panel) and tag-density plot (bottom panel). 'Start' and 'End' mark the coordinates of DNMT3B-peaks. H3K4me3 defines active promoters, H3K79me2+H3K36me3 indicates promoter adjacent exons, and presence of H3K36me3-only labels gene bodies. (**D**) Schematic representation of co-binding by ZBTB24 and DNMT3B at a subset of loci in the genome. (**E**) Quantification of co-bound genes and (**F**) functional pathways regulated by co-bound genes, determined by IPA. (**G**) Changes in expression and (**H**) DNA methylation at ZBTB24-DNMT3B co-bound loci with loss of function of either factor. (**I**) Correlation plot relating changes in expression and changes in methylation (segregated by genomic feature) in the HCT116 DNMT3BKO and ZBTB24 knockdown systems. 5mC changes occurring upon loss-of-function of either factor, within gene bodies, shows the highest correlation (0.55, indicated with red box) suggesting a coordinated role of ZBTB24 and DNMT3B in maintaining gene body DNA methylation.

DISCUSSION

In this study, we investigated the biological role and targeting of ZBTB24, a poorly characterized member of the ZBTB protein family, in a well characterized cell model system for which abundant epigenetic data is available. We map ZBTB24 binding sites in the HCT116 genome and observe its preferential enrichment at active chromatin. We also identify a high confidence DNA recognition motif, which is classified with motifs recognized by the nuclear receptor class family of transcriptional regulators. Using a loss of function approach, we identify ZBTB24 direct and indirect transcriptional targets in HCT116 cells, which highlight ZBTB24's capacity to function as a transcriptional activator or a repressor. ZBTB24 transcriptionally regulates genes related to a diverse group of molecular processes required for maintenance of cellular homeostasis. We also investigated the role of ZBTB24 in modulating DNA methylation and demonstrate genome-wide hypomethylation resulting from ZBTB24 acute depletion. A subset of the ZBTB24-bound genes are co-bound by DNMT3B, implying a coordinated mechanism between the two factors in regulating DNA methylation at specific loci across the genome. This rationale is supported by our observation that ZBTB24 and DNMT3B interact, and that loss of either factor results in deregulated DNA methylation within the bodies of co-bound loci. Furthermore, depletion of ZBTB24 results in reduced DNMT3B occupancy within the bodies of genes cobound by the two factors, suggesting ZBTB24 participates in the recruitement of DNMT3B.

Previously, very little was known about the function of ZBTB24. Since immunodeficiency is one of the major phenotypes of ICF syndrome patients, ZBTB24 was presumed to function as a regulator of B-cell function. ShRNA depletion of ZBTB24 in Burkitt's B-lymphoma Raji cells indeed resulted in cell cycle defects, specifically at the G0/G1 to S phase transition, resulting from activation of IRF2 and BLIMP-1, known inhibitors of B-cell proliferation (24). From studies performed in ES cells derived from a *Zbtb24* BTB-domain deleted mouse model, Wu *et al*. showed that *Cdca7* is a transcriptional target of Zbtb24 and is activated by direct binding at the *Cdca7* promoter (23). Since ZBTB24 is ubiquitously expressed across cell-types as shown here, we reasoned that its functions are unlikely to be restricted to cells of the immune lineage, and thus the use of HCT116 cells would identify ZBTB24's broader role in cellular homeostasis and transcription, and importantly allow us to tap into the wealth of epigenetic information available on HCT116 cells from public databases. ChIP-seq enabled us to identify genes involved in metabolism, chromatin maintenance, and development, in addition to immune function, as targets for ZBTB24 promoter binding. ZBTB24 is bound at the promoters of several crucial regulators of differentiation. HOXB7 for example, coordinates with ERα to drive transcription of ER targets like HER2, MYC and FOS (64) and is a master regulator of proliferation and osteogenesis (41). The classification of the ZBTB24 recognition motif as similar to that of the nuclear receptor class, along with involvement of ZBTB24 transcriptional targets in the VDR/RXR pathway, implies a role for ZBTB24 in transcriptional regulation via nuclear receptor signaling. Members of the nuclear receptor class include hormone receptors and factors that dimerize with retinoic acid receptors to drive pathways crucial for diverse developmental processes (65). In addition to binding at promoter elements, ZBTB24 is also enriched at active and primed enhancers, and at TAD boundaries organized and maintained by CTCF and cohesin. TADs are chromatin microenvironments within which factors interact to bring non-linear genomic regions into close proximity, and serve to regulate intra-TAD activity. It is possible that ZBTB24 is enriched within specific TADS to facilitate interactions between its target genes, or possibly within different regions of a single transcription unit (alone or with DNMT3B), ideas that can be tested in future studies of these factors. Gene promoters robustly bound by ZBTB24 in HCT116 were also enriched for binding in B-cells, suggesting again that the ZBTB24 binding landscape is not restricted to a particular cell-type. However, this needs to be investigated further at a large-scale genomic level across diverse cell-types.

Three of the BTB-family members function as established readers of DNA methylation and coordinate with histone modifying enzymes to bring about changes in transcription. In this study, our data do not support a role for ZBTB24 as a 5mC reader, although we did observe genome-wide loss of DNA methylation resulting from ZBTB24 depletion. Our finding that ZBTB24 co-immunoprecipitates with DNMT3B led us to ask whether ZBTB24 coordinates with DNMT3B in some way to maintain DNA methylation. We indeed observed co-binding of ZBTB24 and DNMT3B at a subset of genes involved in general cellular maintenance; loss of function of either of the factors deregulated gene body methylation suggestive of a coordinated role between the two factors. The mechanism by which the two proteins coordinate to achieve this function remains unknown, however, we hypothesize that promoter-bound ZBTB24 recruits DNMT3B to gene bodies of their target loci and thus acts as a loading factor. This hypothesis is supported by our observation of reduced DNMT3B occupancy resulting from ZBTB24 depletion, within bodies of genes bound by ZBTB24 and DNMT3B (Supplementary Figure S6L). DNA sequences can form loops bringing promoters, enhancers, and downstream exons in close proximity in three-dimensional space (66). CTCF, in addition to mediating long-range chromosomal interactions, also mediates promoter-exon interactions that direct splicing (67). Defects in splicing have been reported in ICF1 patients with *DNMT3B* mutations and in *Dnmt3b*-/- mES cells. Therefore, an alternative mechanism that ZBTB24 and DNMT3B may coordinate their activities is through regulation of interactions within transcription units to modulate expression, intra-domain communication, or alternative mRNA splicing.

In summary, our investigation resulted in the identification of genomic targets of ZBTB24 and highlights its preference for binding within an active chromatin landscape. ZBTB24 acts as an activator or repressor of transcription, a function that likely depends on additional co-factors and/or the local chromatin environment. The similarity of the ZBTB24 recognition motif to the nuclear receptor subclass, and the functional pathways affected upon loss of ZBTB24 function, imply a role for ZBTB24 in reg-

ulating VDR/RXR pathways centered on growth, differentiation, and the interferon response. Finally, we show that ZBTB24 interfaces with DNMT3B at a large set of genes and may recruit DNMT3B to coordinately maintain DNA methylation within gene bodies. Functional outcomes of this interaction will require further investigation but could include chromatin domain organization or regulation of co-transcriptional splicing. One caveat of our study is that the HCT116 cell line exhibits the CpG island methylator phenotype (CIMP) (68), and it is therefore possible that the ZBTB24-DNMT3B regulated 5mC dynamics may be influenced by this property. Velasco *et al*. reported that patients classified as ICF2,3,and 4, but not ICF1 patients, show methylation defects within the CpG poor heterochromatic compartment (69). Although, our findings do not recapitulate this observation, it is likely that the 850K array platform is not ideal for assessing this type of repetitive heterochromatic region originally observed to be targeted for hypomethylation in ICF syndrome (70–72). Extending studies like this into immune cells or ICF2 patient cells will likely be required to firmly identify loci contributing to the immunodeficiency phenotype, something made difficult by the rarity of ICF syndrome patients. Finally, this study adds to the growing link between ZBTB family members and DNA methylation, suggesting that other members of the ZBTB family have similar functions in reading and/or maintaining DNA methylation marks.

DATA AVAILABILITY

The data has been deposited in GEO under accession number GSE111689.

SUPPLEMENTARY DATA

Supplementary Data are available at NAR Online.

ACKNOWLEDGEMENTS

We are grateful to the University of Minnesota Genomics Core for running the RNA-seq and IlluminaMethylation BeadChip EPIC arrays, and the Mayo Clinic Medical Genomic Facility for deep sequencing of ChIP samples. We thank Yuichi Machida for the FLAG-lentiviral vectors and Reeja Maskey for advice on lentiviral experiments. We also thank Bonnie Alver and Ryan Hlady for advice on bioinformatics analyses, and Martin Fernandez-Zapico and Stephanie Safgren for advice on luciferase assays.
Author contributions: J.J.T. designed and performed laboratory experiments as well as bioinformatics analysis and data interpretation, and drafted the manuscript. R.K created ZBTB24 luciferase constructs and performed the luciferase assays. C.P.S provided instructions and advice on processing raw RNA-seq data. J.H.L. conducted library preparation for ChIP-seq. K.K. provided valuable inputs for experimental design. D.Z. assisted with bioinformatic analysis. K.D.R. conceived of the study and its design, assisted with data interpretation, and edited the manuscript.

FUNDING

National Institutes of Health [CA114229 to KDR]; Mayo Clinic Center for Individualized Medicine Epigenomics Program. Funding for open access charge: National Institutes of Health.
Conflict of interest statement. None declared.

REFERENCES

1. Liu,X., Gao,Q., Li,P., Zhao,Q., Zhang,J., Li,J., Koseki,H. and Wong,J. (2013) UHRF1 targets DNMT1 for DNA methylation through cooperative binding of hemi-methylated DNA and methylated H3K9. *Nat. Commun.*, **4**, 1563.
2. Chen,T., Ueda,Y., Dodge,J.E., Wang,Z. and Li,E. (2003) Establishment and maintenance of genomic methylation patterns in mouse embryonic stem cells by Dnmt3a and Dnmt3b. *Mol. Cell. Biol.*, **23**, 5594–5605.
3. Okano,M., Bell,D.W., Haber,D.A. and Li,E. (1999) DNA methyltransferases Dnmt3a and Dnmt3b are essential for de novo methylation and mammalian development. *Cell*, **99**, 247–257.
4. Choi,S.H., Heo,K., Byun,H.M., An,W., Lu,W. and Yang,A.S. (2011) Identification of preferential target sites for human DNA methyltransferases. *Nucleic Acids Res.*, **39**, 104–118.
5. Jin,B., Ernst,J., Tiedemann,R.L., Xu,H., Sureshchandra,S., Kellis,M., Dalton,S., Liu,C., Choi,J.H. and Robertson,K.D. (2012) Linking DNA methyltransferases to epigenetic marks and nucleosome structure genome-wide in human tumor cells. *Cell Rep.*, **2**, 1411–1424.
6. Tiedemann,R.L., Putiri,E.L., Lee,J.H., Hlady,R.A., Kashiwagi,K., Ordog,T., Zhang,Z., Liu,C., Choi,J.H. and Robertson,K.D. (2014) Acute depletion redefines the division of labor among DNA methyltransferases in methylating the human genome. *Cell Rep.*, **9**, 1554–1566.
7. Liao,J., Karnik,R., Gu,H., Ziller,M.J., Clement,K., Tsankov,A.M., Akopian,V., Gifford,C.A., Donaghey,J., Galonska,C. *et al.* (2015) Targeted disruption of DNMT1, DNMT3A and DNMT3B in human embryonic stem cells. *Nat. Genet.*, **47**, 469–478.
8. Velasco,G., Hube,F., Rollin,J., Neuillet,D., Philippe,C., Bouzinba-Segard,H., Galvani,A., Viegas-Pequignot,E. and Francastel,C. (2010) Dnmt3b recruitment through E2F6 transcriptional repressor mediates germ-line gene silencing in murine somatic tissues. *Proc. Natl. Acad. Sci. U.S.A.*, **107**, 9281–9286.
9. Jin,B., Yao,B., Li,J.L., Fields,C.R., Delmas,A.L., Liu,C. and Robertson,K.D. (2009) DNMT1 and DNMT3B modulate distinct polycomb-mediated histone modifications in colon cancer. *Cancer Res.*, **69**, 7412–7421.
10. Baubec,T., Colombo,D.F., Wirbelauer,C., Schmidt,J., Burger,L., Krebs,A.R., Akalin,A. and Schubeler,D. (2015) Genomic profiling of DNA methyltransferases reveals a role for DNMT3B in genic methylation. *Nature*, **520**, 243–247.
11. Neri,F., Rapelli,S., Krepelova,A., Incarnato,D., Parlato,C., Basile,G., Maldotti,M., Anselmi,F. and Oliviero,S. (2017) Intragenic DNA methylation prevents spurious transcription initiation. *Nature*, **543**, 72–77.
12. Gatto,S., Gagliardi,M., Franzese,M., Leppert,S., Papa,M., Cammisa,M., Grillo,G., Velasco,G., Francastel,C., Toubiana,S. *et al.* (2017) ICF-specific DNMT3B dysfunction interferes with intragenic regulation of mRNA transcription and alternative splicing. *Nucleic Acids Res.*, **45**, 5739–5756.
13. Hansen,R.S., Wijmenga,C., Luo,P., Stanek,A.M., Canfield,T.K., Weemaes,C.M. and Gartler,S.M. (1999) The DNMT3B DNA methyltransferase gene is mutated in the ICF immunodeficiency syndrome. *Proc. Natl. Acad. Sci. U.S.A.*, **96**, 14412–14417.
14. Ehrlich,M., Jackson,K. and Weemaes,C. (2006) Immunodeficiency, centromeric region instability, facial anomalies syndrome (ICF). *Orphanet. J. Rare Dis.*, **1**, 2.
15. Hagleitner,M.M., Lankester,A., Maraschio,P., Hulten,M., Fryns,J.P., Schuetz,C., Gimelli,G., Davies,E.G., Gennery,A., Belohradsky,B.H. *et al.* (2008) Clinical spectrum of immunodeficiency, centromeric instability and facial dysmorphism (ICF syndrome). *J. Med. Genet.*, **45**, 93–99.
16. Thijssen,P.E., Ito,Y., Grillo,G., Wang,J., Velasco,G., Nitta,H., Unoki,M., Yoshihara,M., Suyama,M., Sun,Y. *et al.* (2015) Mutations in CDCA7 and HELLS cause immunodeficiency-centromeric instability-facial anomalies syndrome. *Nat. Commun.*, **6**, 7870.

17. Lee,S.U. and Maeda,T. (2012) POK/ZBTB proteins: an emerging family of proteins that regulate lymphoid development and function. *Immunol. Rev.*, **247**, 107–119.
18. Barrilleaux,B.L., Burow,D., Lockwood,S.H., Yu,A., Segal,D.J. and Knoepfler,P.S. (2014) Miz-1 activates gene expression via a novel consensus DNA binding motif. *PLoS One*, **9**, e101151.
19. Walz,S., Lorenzin,F., Morton,J., Wiese,K.E., von Eyss,B., Herold,S., Rycak,L., Dumay-Odelot,H., Karim,S., Bartkuhn,M. *et al.* (2014) Activation and repression by oncogenic MYC shape tumour-specific gene expression profiles. *Nature*, **511**, 483–487.
20. Siggs,O.M. and Beutler,B. (2012) The BTB-ZF transcription factors. *Cell Cycle*, **11**, 3358–3369.
21. Brenner,C., Deplus,R., Didelot,C., Loriot,A., Vire,E., De Smet,C., Gutierrez,A., Danovi,D., Bernard,D., Boon,T. *et al.* (2005) Myc represses transcription through recruitment of DNA methyltransferase corepressor. *EMBO J.*, **24**, 336–346.
22. Fournier,A., Sasai,N., Nakao,M. and Defossez,P.A. (2012) The role of methyl-binding proteins in chromatin organization and epigenome maintenance. *Brief Funct. Genomics*, **11**, 251–264.
23. Wu,H., Thijssen,P.E., de Klerk,E., Vonk,K.K., Wang,J., den Hamer,B., Aytekin,C., van der Maarel,S.M. and Daxinger,L. (2016) Converging disease genes in ICF syndrome: ZBTB24 controls expression of CDCA7 in mammals. *Hum. Mol. Genet.*, **25**, 4041–4051.
24. Liang,J., Yan,R., Chen,G., Feng,J., Wu,W.W., Ren,W., Zhu,C., Zhao,Y., Gao,X.M. and Wang,J. (2016) Downregulation of ZBTB24 hampers the G0/1- to S-phase cell-cycle transition via upregulating the expression of IRF-4 in human B cells. *Genes Immun.*, **17**, 276–282.
25. Rhee,I., Bachman,K.E., Park,B.H., Jair,K.W., Yen,R.W., Schuebel,K.E., Cui,H., Feinberg,A.P., Lengauer,C., Kinzler,K.W. *et al.* (2002) DNMT1 and DNMT3b cooperate to silence genes in human cancer cells. *Nature*, **416**, 552–556.
26. Maskey,R.S., Kim,M.S., Baker,D.J., Childs,B., Malureanu,L.A., Jeganathan,K.B., Machida,Y., van Deursen,J.M. and Machida,Y.J. (2014) Spartan deficiency causes genomic instability and progeroid phenotypes. *Nat. Commun.*, **5**, 5744.
27. Li,H. and Durbin,R. (2009) Fast and accurate short read alignment with Burrows-Wheeler transform. *Bioinformatics*, **25**, 1754–1760.
28. Feng,J., Liu,T., Qin,B., Zhang,Y. and Liu,X.S. (2012) Identifying ChIP-seq enrichment using MACS. *Nat. Protoc.*, **7**, 1728–1740.
29. Bailey,T.L., Boden,M., Buske,F.A., Frith,M., Grant,C.E., Clementi,L., Ren,J., Li,W.W. and Noble,W.S. (2009) MEME SUITE: tools for motif discovery and searching. *Nucleic Acids Res.*, **37**, W202–W208.
30. Ramirez,F., Dundar,F., Diehl,S., Gruning,B.A. and Manke,T. (2014) deepTools: a flexible platform for exploring deep-sequencing data. *Nucleic Acids Res.*, **42**, W187–W191.
31. Pertea,M., Kim,D., Pertea,G.M., Leek,J.T. and Salzberg,S.L. (2016) Transcript-level expression analysis of RNA-seq experiments with HISAT, StringTie and Ballgown. *Nat. Protoc.*, **11**, 1650–1667.
32. Han,B.Y., Foo,C.S., Wu,S. and Cyster,J.G. (2016) The C2H2-ZF transcription factor Zfp335 recognizes two consensus motifs using separate zinc finger arrays. *Genes Dev.*, **30**, 1509–1514.
33. de Greef,J.C., Wang,J., Balog,J., den Dunnen,J.T., Frants,R.R., Straasheijm,K.R., Aytekin,C., van der Burg,M., Duprez,L., Ferster,A. *et al.* (2011) Mutations in ZBTB24 are associated with immunodeficiency, centromeric instability, and facial anomalies syndrome type 2. *Am. J. Hum. Genet.*, **88**, 796–804.
34. Spector,D.L. and Lamond,A.I. (2011) Nuclear speckles. *Cold Spring Harb. Perspect. Biol.*, **3**, a000646.
35. King,A.D., Huang,K., Rubbi,L., Liu,S., Wang,C.Y., Wang,Y., Pellegrini,M. and Fan,G. (2016) Reversible regulation of promoter and enhancer histone landscape by DNA methylation in mouse embryonic stem cells. *Cell Rep.*, **17**, 289–302.
36. Ernst,J. and Kellis,M. (2017) Chromatin-state discovery and genome annotation with ChromHMM. *Nat. Protoc.*, **12**, 2478–2492.
37. Hata,K., Takashima,R., Amano,K., Ono,K., Nakanishi,M., Yoshida,M., Wakabayashi,M., Matsuda,A., Maeda,Y., Suzuki,Y. *et al.* (2013) Arid5b facilitates chondrogenesis by recruiting the histone demethylase Phf2 to Sox9-regulated genes. *Nat. Commun.*, **4**, 2850.
38. Archer,N.P., Perez-Andreu,V., Stoltze,U., Scheurer,M.E., Wilkinson,A.V., Lin,T.N., Qian,M., Goodings,C., Swartz,M.D., Ranjit,N. *et al.* (2017) Family-based exome-wide association study of childhood acute lymphoblastic leukemia among Hispanics confirms role of ARID5B in susceptibility. *PLoS One*, **12**, e0180488.
39. Kreile,M., Rots,D., Zarina,A., Rautiainen,L., Visnevska-Preciniece,Z., Kovalova,Z. and Gailite,L. (2018) Association of ARID5B genetic variants with risk of childhood B cell precursor Acute Lymphoblastic Leukaemia in Latvia. *Asian Pac. J. Cancer Prev.*, **19**, 91–95.
40. Urayama,K.Y., Takagi,M., Kawaguchi,T., Matsuo,K., Tanaka,Y., Ayukawa,Y., Arakawa,Y., Hasegawa,D., Yuza,Y., Kaneko,T. *et al.* (2018) Regional evaluation of childhood acute lymphoblastic leukemia genetic susceptibility loci among Japanese. *Sci. Rep.*, **8**, 789.
41. Candini,O., Spano,C., Murgia,A., Grisendi,G., Veronesi,E., Piccinno,M.S., Ferracin,M., Negrini,M., Giacobbi,F., Bambi,F. *et al.* (2015) Mesenchymal progenitors aging highlights a miR-196 switch targeting HOXB7 as master regulator of proliferation and osteogenesis. *Stem Cells*, **33**, 939–950.
42. Poulsen,M., Lukas,C., Lukas,J., Bekker-Jensen,S. and Mailand,N. (2012) Human RNF169 is a negative regulator of the ubiquitin-dependent response to DNA double-strand breaks. *J. Cell Biol.*, **197**, 189–199.
43. Magnani,R., Dirk,L.M., Trievel,R.C. and Houtz,R.L. (2010) Calmodulin methyltransferase is an evolutionarily conserved enzyme that trimethylates Lys-115 in calmodulin. *Nat. Commun.*, **1**, 43.
44. Jho,E.H., Zhang,T., Domon,C., Joo,C.K., Freund,J.N. and Costantini,F. (2002) Wnt/beta-catenin/Tcf signaling induces the transcription of Axin2, a negative regulator of the signaling pathway. *Mol. Cell. Biol.*, **22**, 1172–1183.
45. Hansen,A.S., Pustova,I., Cattoglio,C., Tjian,R. and Darzacq,X. (2017) CTCF and cohesin regulate chromatin loop stability with distinct dynamics. *Elife*, **6**, e25776.
46. Sun,Y.M., Cooper,M., Finch,S., Lin,H.H., Chen,Z.F., Williams,B.P. and Buckley,N.J. (2008) Rest-mediated regulation of extracellular matrix is crucial for neural development. *PLoS One*, **3**, e3656.
47. Martin,D. and Grapin-Botton,A. (2017) The importance of REST for development and function of beta cells. *Front. Cell Dev. Biol.*, **5**, 12.
48. Xin,M., Davis,C.A., Molkentin,J.D., Lien,C.L., Duncan,S.A., Richardson,J.A. and Olson,E.N. (2006) A threshold of GATA4 and GATA6 expression is required for cardiovascular development. *Proc. Natl. Acad. Sci. U.S.A.*, **103**, 11189–11194.
49. Koutsourakis,M., Langeveld,A., Patient,R., Beddington,R. and Grosveld,F. (1999) The transcription factor GATA6 is essential for early extraembryonic development. *Development*, **126**, 723–732.
50. Carlin,A.F., Plummer,E.M., Vizcarra,E.A., Sheets,N., Joo,Y., Tang,W., Day,J., Greenbaum,J., Glass,C.K., Diamond,M.S. *et al.* (2017) An IRF-3-, IRF-5-, and IRF-7-independent pathway of dengue viral resistance utilizes IRF-1 to stimulate type I and II interferon responses. *Cell Rep.*, **21**, 1600–1612.
51. Lazear,H.M., Lancaster,A., Wilkins,C., Suthar,M.S., Huang,A., Vick,S.C., Clepper,L., Thackray,L., Brassil,M.M., Virgin,H.W. *et al.* (2013) IRF-3, IRF-5, and IRF-7 coordinately regulate the type I IFN response in myeloid dendritic cells downstream of MAVS signaling. *PLoS Pathog.*, **9**, e1003118.
52. Groner,A.C., Cato,L., de Tribolet-Hardy,J., Bernasocchi,T., Janouskova,H., Melchers,D., Houtman,R., Cato,A.C.B., Tschopp,P., Gu,L. *et al.* (2016) TRIM24 Is an oncogenic transcriptional activator in prostate cancer. *Cancer Cell*, **29**, 846–858.
53. Tisserand,J., Khetchoumian,K., Thibault,C., Dembele,D., Chambon,P. and Losson,R. (2011) Tripartite motif 24 (Trim24/Tif1alpha) tumor suppressor protein is a novel negative regulator of interferon (IFN)/signal transducers and activators of transcription (STAT) signaling pathway acting through retinoic acid receptor alpha (Raralpha) inhibition. *J. Biol. Chem.*, **286**, 33369–33379.
54. Sato,R., Shibata,T., Tanaka,Y., Kato,C., Yamaguchi,K., Furukawa,Y., Shimizu,E., Yamaguchi,R., Imoto,S., Miyano,S. *et al.* (2017) Requirement of glycosylation machinery in TLR responses revealed by CRISPR/Cas9 screening. *Int. Immunol.*, **29**, 347–355.
55. Filion,G.J., Zhenilo,S., Salozhin,S., Yamada,D., Prokhortchouk,E. and Defossez,P.A. (2006) A family of human zinc finger proteins that bind methylated DNA and repress transcription. *Mol. Cell. Biol.*, **26**, 169–181.
56. Pozner,A., Hudson,N.O., Trewhella,J., Terooatea,T.W., Miller,S.A. and Buck-Koehntop,B.A. (2018) The C-terminal zinc fingers of

ZBTB38 are novel selective readers of DNA methylation. *J. Mol. Biol.*, **430**, 258–271.
57. Prokhortchouk,A., Hendrich,B., Jorgensen,H., Ruzov,A., Wilm,M., Georgiev,G., Bird,A. and Prokhortchouk,E. (2001) The p120 catenin partner Kaiso is a DNA methylation-dependent transcriptional repressor. *Genes Dev.*, **15**, 1613–1618.
58. Tiedemann,R.L., Hlady,R.A., Hanavan,P.D., Lake,D.F., Tibes,R., Lee,J.H., Choi,J.H., Ho,T.H. and Robertson,K.D. (2016) Dynamic reprogramming of DNA methylation in SETD2-deregulated renal cell carcinoma. *Oncotarget*, **7**, 1927–1946.
59. Zhou,D., Alver,B.M., Li,S., Hlady,R.A., Thompson,J.J., Schroeder,M.A., Lee,J.H., Qiu,J., Schwartz,P.H., Sarkaria,J.N. *et al.* (2018) Distinctive epigenomes characterize glioma stem cells and their response to differentiation cues. *Genome Biol.*, **19**, 43.
60. Huff,J.T., Plocik,A.M., Guthrie,C. and Yamamoto,K.R. (2010) Reciprocal intronic and exonic histone modification regions in humans. *Nat. Struct. Mol. Biol.*, **17**, 1495–1499.
61. ENCODE Project Consortium. (2012) An integrated encyclopedia of DNA elements in the human genome. *Nature*, **489**, 57–74.
62. Bannister,A.J., Schneider,R., Myers,F.A., Thorne,A.W., Crane-Robinson,C. and Kouzarides,T. (2005) Spatial distribution of di- and tri-methyl lysine 36 of histone H3 at active genes. *J. Biol. Chem.*, **280**, 17732–17736.
63. Edmunds,J.W., Mahadevan,L.C. and Clayton,A.L. (2008) Dynamic histone H3 methylation during gene induction: HYPB/Setd2 mediates all H3K36 trimethylation. *EMBO J.*, **27**, 406–420.
64. Jin,K., Park,S., Teo,W.W., Korangath,P., Cho,S.S., Yoshida,T., Gyorffy,B., Goswami,C.P., Nakshatri,H., Cruz,L.A. *et al.* (2015) HOXB7 Is an ERalpha cofactor in the activation of HER2 and multiple ER target genes leading to endocrine resistance. *Cancer Discov.*, **5**, 944–959.
65. Huang,P., Chandra,V. and Rastinejad,F. (2014) Retinoic acid actions through mammalian nuclear receptors. *Chem. Rev.*, **114**, 233–254.
66. Mercer,T.R., Edwards,S.L., Clark,M.B., Neph,S.J., Wang,H., Stergachis,A.B., John,S., Sandstrom,R., Li,G., Sandhu,K.S. *et al.* (2013) DNase I-hypersensitive exons colocalize with promoters and distal regulatory elements. *Nat. Genet.*, **45**, 852–859.
67. Ruiz-Velasco,M., Kumar,M., Lai,M.C., Bhat,P., Solis-Pinson,A.B., Reyes,A., Kleinsorg,S., Noh,K.M., Gibson,T.J. and Zaugg,J.B. (2017) CTCF-mediated chromatin loops between promoter and gene body regulate alternative splicing across individuals. *Cell Syst.*, **5**, 628–637.
68. Ahmed,D., Eide,P.W., Eilertsen,I.A., Danielsen,S.A., Eknaes,M., Hektoen,M., Lind,G.E. and Lothe,R.A. (2013) Epigenetic and genetic features of 24 colon cancer cell lines. *Oncogenesis*, **2**, e71.
69. Velasco,G., Grillo,G., Touleimat,N., Ferry,L., Ivkovic,I., Ribierre,F., Deleuze,J.-F., Chantalat,S., Picard,C. and Francastel,C. (2018) Comparative methylome analysis of ICF patients identifies heterochromatin loci that require ZBTB24, CDCA7 and HELLS for their methylated state. *Hum. Mol. Genet.*, **27**, 2409–2424.
70. Luciani,J.J., Depetris,D., Missirian,C., Mignon-Ravix,C., Metzler-Guillemain,C., Megarbane,A., Moncla,A. and Mattei,M.G. (2005) Subcellular distribution of HP1 proteins is altered in ICF syndrome. *Eur. J. Hum. Genet.*, **13**, 41–51.
71. Yehezkel,S., Segev,Y., Viegas-Pequignot,E., Skorecki,K. and Selig,S. (2008) Hypomethylation of subtelomeric regions in ICF syndrome is associated with abnormally short telomeres and enhanced transcription from telomeric regions. *Hum. Mol. Genet.*, **17**, 2776–2789.
72. Jiang,Y.L., Rigolet,M., Bourc'his,D., Nigon,F., Bokesoy,I., Fryns,J.P., Hulten,M., Jonveaux,P., Maraschio,P., Megarbane,A. *et al.* (2005) DNMT3B mutations and DNA methylation defect define two types of ICF syndrome. *Hum. Mutat.*, **25**, 56–63.